

- [44] Woodward DF, Nieves AL, Spada CS, Williams LS, Tuckett RP. Characterization of a behavioral model for peripherally evoked itch suggests platelet-activating factor as a potent pruritogen. *J Pharmacol Exp Ther* 1995;272:758.
- [45] Hattori M, Adachi H, Tsujimoto M, Arai H, Inoue K. Miller–Dieker lissencephaly gene encodes a subunit of brain platelet-activating factor acetylhydrolase. *Nature* 1994;370:216.
- [46] Hirotsune S, Fleck MW, Gambello MJ, Bix GJ, Chen A, Clark GD, et al. Graded reduction of Pafah1b1 (Lis1) activity results in neuronal migration defects and early embryonic lethality. *Nat Genet* 1998;19:333.
- [47] Ishii S, Nagase T, Tashiro F, Ikuta K, Sato S, Waga I, et al. Bronchial hyperreactivity, increased endotoxin lethality and melanocytic tumorigenesis in transgenic mice overexpressing platelet-activating factor receptor. *EMBO J* 1997;16:133.
- [48] Araki K, Araki M, Miyazaki J, Vassalli P. Site-specific recombination of a transgene in fertilized eggs by transient expression of Cre recombinase. *Proc Natl Acad Sci USA* 1995;92:160.
- [49] Sunaga S, Maki K, Komagata Y, Ikuta K, Miyazaki JI. Efficient removal of loxP-flanked DNA sequences in a gene-targeted locus by transient expression of Cre recombinase in fertilized eggs. *Mol Reprod Dev* 1997;46:109.
- [50] Sakai K, Miyazaki JI. A transgenic mouse line that retains Cre recombinase activity in mature oocytes irrespective of the cre transgene transmission. *Biochem Biophys Res Commun* 1997;237:318.
- [51] Ishii S, Kuwaki T, Nagase T, Maki K, Tashiro F, Sunaga S, et al. Impaired anaphylactic responses with intact sensitivity to endotoxin in mice lacking a platelet-activating factor receptor. *J Exp Med* 1998;187:1779.
- [52] Aihara M, Ishii S, Kume K, Shimizu T. Interaction between neurone and microglia mediated by platelet-activating factor. *Genes Cells* 2000;5:397.
- [53] Barbuti A, Ishii S, Shimizu T, Robinson RB, Feinmark SJ. Block of the background K⁺ channel, TASK-1, contributes to the arrhythmogenic effects of platelet-activating factor. *Am J Physiol* 2002;282:2024.
- [54] Wu C, Stojanov T, Chami O, Ishii S, Shimizu T, Li A, et al. Evidence for the autocrine induction of capacitation of mammalian spermatozoa. *J Biol Chem* 2001;276:26962.
- [55] Nagase T, Ishii S, Katayama H, Fukuchi Y, Ouchi Y, Shimizu T. Airway responsiveness in transgenic mice overexpressing platelet-activating factor receptor: roles of thromboxanes and leukotrienes. *Am J Respir Crit Care Med* 1997;156:1621.
- [56] Nagase T, Ishii S, Shindou H, Ouchi Y, Shimizu T. Airway hyperresponsiveness in transgenic mice overexpressing platelet activating factor receptor is mediated by an atropine-sensitive pathway. *Am J Respir Crit Care Med* 2002;165:200.
- [57] Wu T, Rieves RD, Logun C, Shelhamer JH. Platelet-activating factor stimulates eicosanoid production in cultured feline tracheal epithelial cells. *Lung* 1995;173:89.
- [58] Gomez FP, Iglesia R, Roca J, Barbera JA, Chung KF, Rodriguez- Roisin R. The effects of 5-lipoxygenase inhibition by zileuton on platelet-activating-factor-induced pulmonary abnormalities in mild asthma. *Am J Respir Crit Care Med* 1998;157:1559.
- [59] Nagase T, Ishii S, Kume K, Uozumi N, Izumi T, Ouchi Y, et al. Platelet-activating factor mediates acid-induced lung injury in genetically-engineered mice. *J Clin Invest* 1999;104:1071.
- [60] Koltai M, Hosford D, Braquet P. PAF-induced amplification of mediator release in septic shock: prevention or downregulation by PAF antagonists. *J Lipid Mediat* 1993;6:183.
- [61] Kobayashi K, Ishii S, Kume K, Takahashi T, Shimizu T, Manabe T. Platelet-activating factor receptor is not required for long-term potentiation in the hippocampal CA1 region. *Eur J Neurosci* 1999;11:1313.
- [62] Chen C, Magee JC, Marcheselli V, Hardy M, Bazan NG. Attenuated LTP in hippocampal dentate gyrus neurons of mice deficient in the PAF receptor. *J Neurophysiol* 2001;85:384.
- [63] Sato S, Kume K, Ito C, Ishii S, Shimizu T. Accelerated proliferation of the epidermal keratinocytes by the transgenic expression of the platelet-activating factor receptor. *Arch Dermatol Res* 1999;291:614.
- [64] Halaban R, Langdon R, Birchall N, Cuono C, Baird A, Scott G, et al. Basic fibroblast growth factor from human keratinocytes is a natural mitogen for melanocytes. *J Cell Biol* 1988;107:1611.
- [65] Imokawa G, Miyagishi M, Yada Y. Endothelin-1 as a new melanogen: coordinated expression of its gene and the tyrosinase gene in UVB-exposed human epidermis. *J Invest Dermatol* 1995;105:32.
- [66] Grabbe J, Welker P, Dippel E, Czarnetzki BM. Stem cell factor, a novel cutaneous growth factor for mast cells and melanocytes. *Arch Dermatol Res* 1994;287:78.
- [67] Ishibashi S, Brown MS, Goldstein JL, Gerard RD, Hammer RE, Herz J. Hypercholesterolemia in low density lipoprotein receptor knockout mice and its reversal by adenovirus-mediated gene delivery. *J Clin Invest* 1993;92:883.

- [68] Gurney AL, Carver-Moore K, de Sauvage FJ, Moore MW. Thrombocytopenia in c-mpl-deficient mice. *Science* 1994;265:1445.
- [69] Shindou H, Ishii S, Uozumi N, Shimizu T. Roles of cytosolic phospholipase A2 and platelet-activating factor receptor in the Ca-induced biosynthesis of PAF. *Biochem Biophys Res Commun* 2000;271:812.
- [70] Ohshima N, Ishii S, Izumi T, Shimizu T. Receptor-dependent metabolism of platelet-activating factor in murine macrophages. *J Biol Chem* 2002;277:9722.
- [71] Saeed SA, Simjee RU, Mahmood F, Rahman NN. Dual inhibition of platelet-activating factor and arachidonic acid metabolism by ajmaline and effect on carrageenan-induced rat paw oedema. *J Pharm Pharmacol* 1993;45:715.
- [72] Hsiao G, Ko FN, Jong TT, Teng CM. Antiplatelet action of 3',4'-diisovalerylhellactone diester purified from *Peucedanum japonicum*. *Thunb Biol Pharm Bull* 1998;21:688.
- [73] Le Texier L, Favre E, Redeuilh C, Blavet N, Bellahsene T, Dive G, et al. Structure-activity relationships in platelet-activating factor (PAF). 7. Tetrahydrofuran derivatives as dual PAF antagonists and acetylcholinesterase inhibitors: synthesis and PAF-antagonistic activity. *J Lipid Mediat Cell Signal* 1996;13:189.
- [74] Svetlov SI, Howard KM, Miwa M, Flickinger BD, Olson MS. Interaction of platelet-activating factor with rat hepatocytes: uptake, translocation, metabolism, and effects on PAF-acetylhydrolase secretion and protein tyrosine phosphorylation. *Arch Biochem Biophys* 1996;327:113.
- [75] Adachi T, Aoki J, Many H, Asou H, Arai H, Inoue K. PAF analogues capable of inhibiting PAF acetylhydrolase activity suppress migration of isolated rat cerebellar granule cells. *Neurosci Lett* 1997;235:133.
- [76] Piwinski JJ, Wong JK, Green MJ, Ganguly AK, Billah MM, West RJ, et al. Dual antagonists of platelet activating factor and histamine: identification of structural requirements for dual activity of *N*-acyl-4-(5,6-dihydro-11*H*-benzo [5,6]cyclohepta-[1,2-*b*]pyridin-11-ylidene)piperidines. *J Med Chem* 1991;34:457.
- [77] Billah MM, Egan RW, Ganguly AK, Green MJ, Kreutner W, Piwinski JJ, et al. Discovery and preliminary pharmacology of Sch 37370, a dual antagonist of PAF and histamine. *Lipids* 1991;26:1172.
- [78] Merlos M, Giral M, Balsa D, Ferrando R, Queralt M, Puigdemont A, et al. Rupatadine, a new potent, orally active dual antagonist of histamine and platelet-activating factor (PAF). *J Pharmacol Exp Ther* 1997;280:114.

Ginkgolide Derivatives for Photolabeling Studies: Preparation and Pharmacological Evaluation

Kristian Strømgaard,[†] D. Roland Saito,[†] Hideo Shindou,[‡] Satoshi Ishii,[‡] Takao Shimizu,[‡] and Koji Nakanishi^{*†}

Department of Chemistry, Columbia University, 3000 Broadway, New York, New York 10027,

Department of Biochemistry and Molecular Biology, Faculty of Medicine, The University of Tokyo, Hongo 7-3-1, Bunkyo-ku, Tokyo 113-0033, Japan, and CREST of Japan Science and Technology Corporation, Tokyo 113-0033, Japan

Received April 4, 2002

The terpene trilactones (TTLs), ginkgolides and bilobalide, are structurally unique constituents of *Ginkgo biloba* extracts, which exhibit various neuromodulatory properties. Although the TTLs are believed to be responsible for some of these effects, the specific interactions with targets in the central nervous system remain to be elucidated on a molecular level. Ginkgolides are known antagonists of the platelet-activating factor (PAF) receptor. Herein, we describe the first examination of the binding of native TTLs and their derivatives to the cloned PAF receptor, confirming that of the TTLs, ginkgolide B is the most potent PAF receptor antagonist. Ginkgolide derivatives carrying photoactivatable and fluorescent groups for the purpose of performing photolabeling have been prepared and evaluated using the cloned PAF receptor. These studies have shown that ginkgolide derivatives with aromatic photoactivatable substituents are potent PAF receptor antagonists with K_i values of 0.09–0.79 μM and hence excellent ligands for clarifying the binding of ginkgolides to PAF receptor by photolabeling studies. Ginkgolide derivatives incorporating both fluorescent and photoactivatable groups still retained binding affinity to the PAF receptor and hence should be promising ligands for photolabeling and subsequent sequencing studies.

Introduction

Ginkgo biloba L., the last surviving member of a family of trees (*Ginkgoaceae*) that appeared more than 250 million years ago, has been mentioned in the Chinese Materia Medica for more than 2500 years.¹ A number of *G. biloba* natural products have been isolated,² the most unique being the terpene trilactones (TTLs), i.e., ginkgolides A, B, C, J, and M (1–5) and bilobalide (6) (Figure 1).^{3–6} The ginkgolides are diterpenes with a cage skeleton consisting of six five-membered rings, i.e., a spiro[4.4]nonane carbocycle, three lactones, and a tetrahydrofuran (THF). The difference between the five ginkgolides lies in the variation in the number and positions of hydroxyl groups on the spirononane framework (Figure 1).

A standardized *G. biloba* extract (EGb 761) containing TTLs (5–7%) and flavonoids (22–24%) has demonstrated neuromodulatory properties,⁷ and several clinical studies using EGb 761 have reported positive effects on various neurodegenerative diseases,^{8–13} including Alzheimer's disease (AD).^{14,15} A recent study by Schultz and co-workers found that EGb 761 upregulated several genes in rat hippocampus and cortex, including genes expressing proteins such as transthyretin and neuronal tyrosine/threonine phosphatase, both of which are believed to be involved in AD.¹⁶ Several recent studies on healthy volunteers have shown positive effects of EGb 761 on short-term working memory indicating that

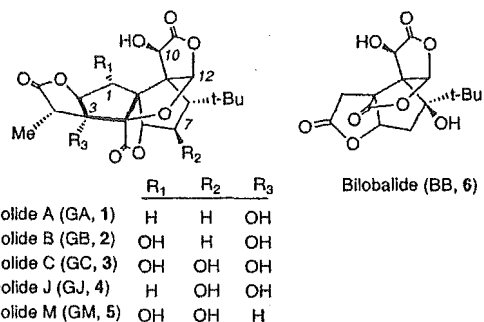


Figure 1. TTLs isolated from *G. biloba*. GA (1), GB (2), and GC (3) are found in the leaves and root bark of *G. biloba*, but GJ (4) is found only in the leaves, and GM (5) is found only in the root bark.

constituents of *G. biloba* also influence the brain under physiological conditions.^{17–20}

Although the molecular basis for the action of *G. biloba* TTL constituents on the central nervous system (CNS) is only poorly understood, it is known that the ginkgolides, particularly ginkgolide B (GB, 2), is a potent in vitro antagonist of the platelet-activating factor receptor (PAFR).²¹ PAF (1-*O*-alkyl-2-acetyl-sn-glycero-3-phosphocholine, Figure 2) is a phospholipid mediator involved in numerous disorders including acute allergy, inflammation, asthma, and ischemic injury. These effects are manifested through binding of PAF to the PAFR, a G protein-coupled receptor that is found in organs such as the lungs, liver, kidneys,^{22–24} and brain.^{25,26} The function of PAF in the brain is still not clear, although PAF has been suggested to play a role in diseases of aging²⁷ and in initiating human immunodeficiency virus (HIV)-related neuropathogenesis.²⁸ PAF has also been suggested as a retrograde

* To whom correspondence should be addressed. Tel: +1 212 854 2169. Fax: +1 212 932 8273. E-mail: kn5@columbia.edu.

[†] Columbia University.

[‡] The University of Tokyo and CREST of Japan Science and Technology Corp.

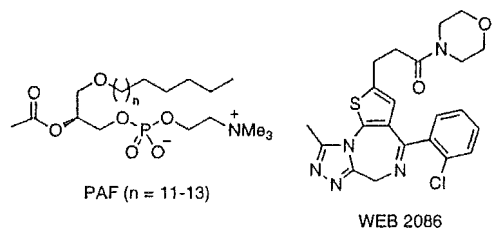


Figure 2. Structures of PAF, the endogenous ligand for the PAFR, and WEB 2086, a potent and selective antagonist, both of which have been used in radioligand binding studies.

messenger in long-term potentiation (LTP).^{29,30} However, studies using PAFR knock-out mice gave contradictory results; one study showed attenuation of LTP in the hippocampal dentate gyrus regions of mice lacking the PAFR,³¹ whereas another study showed that the PAFR was not required for LTP in the hippocampal CA1 region.³² These discrepancies may be due to differences in the hippocampal areas observed, as well as the assay conditions used. However, it is still unclear whether the neuromodulatory effect of TTLs or *G. biloba* extract is related to the PAFR.^{33,34}

With few exceptions, previous structure–activity relationship (SAR) studies of TTLs on the PAFR have focused almost entirely on derivatives of GB (2). In all cases, the derivatives were evaluated for their ability to prevent PAF-induced aggregation of rabbit platelets. Corey et al. investigated various intermediates encountered during the course of the total syntheses of ginkgolide A (GA, 1),³⁵ GB (2),³⁶ and bilobalide (BB, 6)³⁷ and found that although the terminal methyl-bearing lactone was not essential for activity and could be replaced by other lipophilic groups,³⁸ the *tert*-butyl group was important for PAFR antagonism.³⁹ Park et al. synthesized over 200 derivatives of GB (2), with particular focus on aromatic substituents at 10-OH, and found most of them to be more potent than the parent compound.⁴⁰ Similar derivatives recently synthesized by Hu et al. also yielded compounds more potent than GB (2),^{41,42} whereas other variations in GA (1) and GB (2) led to a decrease in activity.^{43,44}

In the following, we describe the first evaluation of the interaction of all native ginkgolides and bilobalide with the cloned PAFR by a radioligand binding assay, as well as their functional properties by intracellular calcium measurements. A series of ginkgolide derivatives with photoactivatable and fluorescent groups have

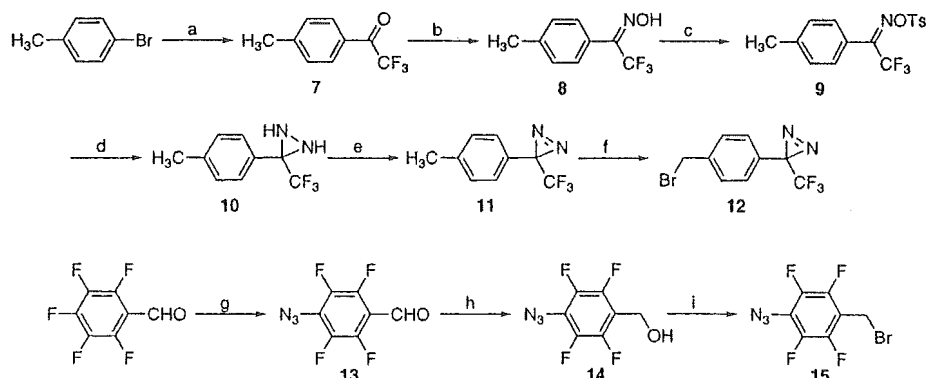
been prepared, and these analogues have been assessed for their ability to displace radioligand binding to cloned PAFR.

Results

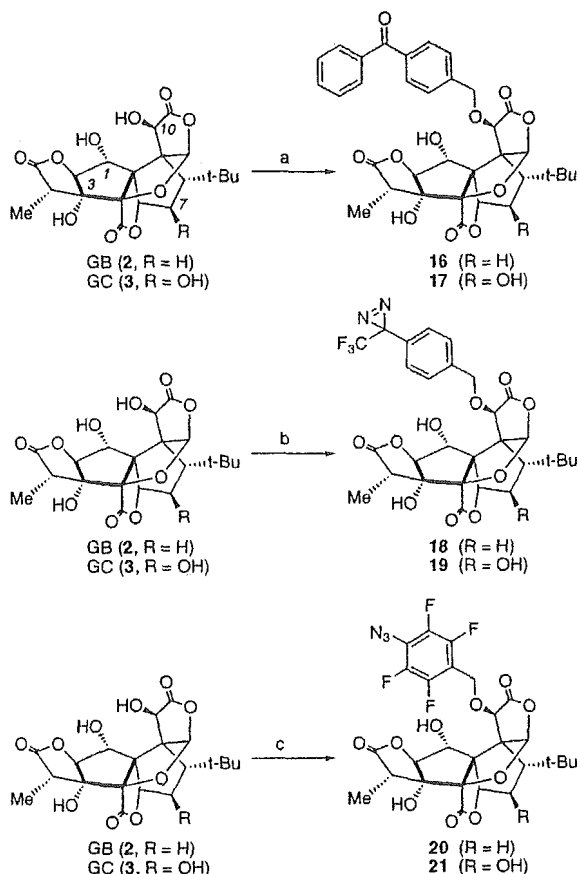
Synthesis. A series of photoactivatable GB (2) and ginkgolide C (GC, 3) derivatives were designed based on previous SAR studies of ginkgolides, which demonstrated that bulky aromatic substituents in the 10-OH position of GB (2) increase activity at the PAFR.^{40–42} Three different photoactivatable moieties, benzophenone, trifluoromethyl-diazirine, and tetrafluorophenyl azide, were chosen as they have been described as being among the most successful for labeling receptors and enzymes.^{45–47} Most importantly, upon irradiation, these photoactivatable groups react with the receptor via different intermediates, namely, a radical, a carbene, or a (singlet) nitrene for the benzophenone, trifluoromethyl-diazirine, and tetrafluorophenyl azide moieties, respectively.⁴⁵ Because it is essentially impossible to predict which group will be most readily incorporated into the receptor, use of these different groups increases the likelihood of a successful incorporation.

4-(Bromomethyl)benzophenone was commercially available, whereas trifluoromethyl-diazirine 12^{48,49} and tetrafluorophenyl azide 15^{50–52} were synthesized, respectively, as outlined in Scheme 1. The bromotrifluoromethyl-diazirine 12 was synthesized starting from readily available 4-bromotoluene, which was reacted with *N*-trifluoroacetyl-piperidine⁴⁸ to give trifluoroacetyl toluene 7. The trifluoroacetyl compound 7 was then reacted with hydroxylamine hydrochloride in pyridine to form oxime 8. Reacting the latter with *p*-toluenesulfonyl chloride led to the tosylated oxime 9, which was placed in a thick-walled screw-capped flask and reacted overnight with liquid ammonia in diethyl ether to form the diaziridine 10; under dim red light, diaziridine 10 was oxidized with iodine to give methylphenyl-trifluoromethyl-diazirine 11. Finally, 11 was brominated with *N*-bromosuccinimide (NBS) using a catalytic amount of 2,2'-azobisisobutyronitrile (AIBN) to form 3-(4-bromomethylphenyl)-3-trifluoromethyl-3*H*-diazirine (12, Scheme 1). Benzoyl peroxide was initially used as a radical initiator, but the reaction yielded multiple products resulting from multiple bromine substitutions. The use of AIBN led to a 4:1 ratio of monobrominated 12 and geminal dibromosubstituted methylphenyl-trifluoromethyl-diazirine, but

Scheme 1^a



^a Reagents: (a) *N*-Trifluoroacetyl-piperidine, *n*-butyllithium. (b) Hydroxylamine. (c) *p*-Toluenesulfonyl chloride, pyridine. (d) NH_3 . (e) I_2 , Et_3N . (f) NBS, AIBN. (g) NaN_3 . (h) Me_2NHBH_3 . (i) PBr_3 .

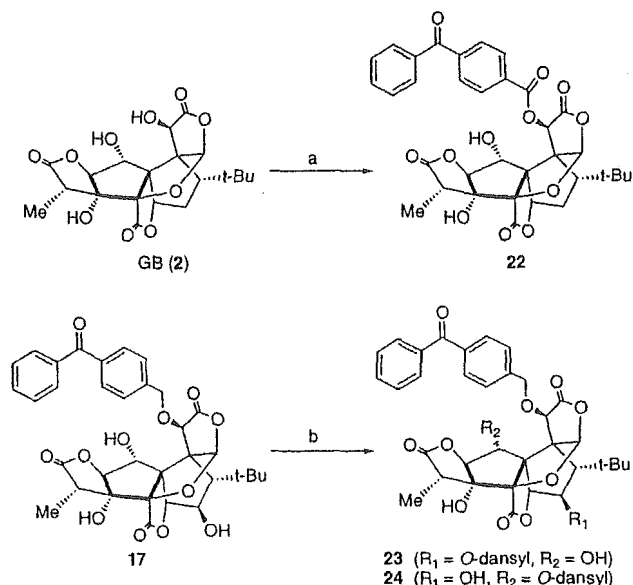
Scheme 2^a

^a Reagents: (a) 4-(Bromomethyl)benzophenone, KH. (b) Compound **12**, KH. (c) Compound **15**, KH.

separation of the two products required several repetitions of flash column chromatography to yield the monobromo-substituted diazirine **12** in sufficient purity.

For the synthesis of tetrafluorophenyl azide **15**, pentafluorobenzaldehyde was heated with sodium azide in an acetone–water mixture. Because pentafluorophenyl groups that contain electron-withdrawing groups undergo nucleophilic aromatic substitution regioselectively in the para position, azidophenylaldehyde **13** was obtained in high yield, and no ortho-substituted product was observed. Aldehyde **13** was selectively reduced with a dimethylamine–borane complex to form the benzyl alcohol **14**. The benzyl alcohol **14** was then brominated by refluxing with phosphorus tribromide in pyridine and chloroform to give the desired product **15** (Scheme 1).

Preparation of GB and GC derivatives **16–21** was performed by reacting GB (**2**) and GC (**3**) with 4-(bromomethyl)benzophenone, 3-(4-bromomethylphenyl)-3-trifluoromethyl-3*H*-diazirine (**12**), and 1-azido-4-(bromomethyl)-2,3,5,6-tetrafluorobenzene (**15**), respectively (Scheme 2). Ginkgolides GB (**2**) and GC (**3**) were derivatized almost exclusively at 10-OH when potassium hydride (KH) was used as base, as was previously shown for GB (**2**),⁴⁰ whereas other bases were less selective, giving rise to products derivatized at 1-OH as well. It is noteworthy that 7-OH present in GC (**3**) does not react under any of the above-mentioned reaction conditions. Generally, the position of the substituent was determined from the ¹H NMR coupling of appropriate protons in dimethyl sulfoxide (DMSO)-*d*₆, as well as by correlation spectroscopy (COSY) spectra. The

Scheme 3^a

^a Reagents: (a) 4-Benzoylbenzoic acid, EDC, DMAP. (b) Dansyl chloride, DMAP.

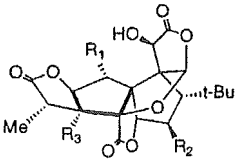
relative chemical shift of 12-H in DMSO-*d*₆ can also be used in differentiating 1- and 10-OH substitutions.⁴²

The coupling of GB (**2**) with 4-benzoylbenzoic acid using 1-[3-(dimethylamino)propyl]-3-ethylcarbodiimide HCl (EDC) and 4-(dimethylamino)pyridine (DMAP) occurred exclusively at 10-OH to give 10-benzophenonecarbonyl GB (**22**) in good yield (Scheme 3). In 10-benzophenonecarbonyl GB (**22**), the photoactivatable benzophenone moiety is linked to the ginkgolide skeleton through an ester linkage. After it is incorporated into the receptor, the ester group can be aminolyzed with a fluorescent amine such as 1-pyrenemethylamine, thus avoiding the use of radioactivity for photolabeling and sequencing.⁵⁴

GC derivatives **17**, **19**, and **21** can be reacted further to incorporate fluorescent groups; for example, benzophenone derivative **17** was reacted with 1 equiv of 5-(dimethylamino)naphthalene-sulfonyl (dansyl) chloride to give 10-*O*-benzophenone-7-*O*-dansyl GC (**23**) with almost exclusive reaction at 7-OH (Scheme 3). Interestingly, increasing the amount of dansyl chloride to 2 equiv gave 10-*O*-benzophenone-1-*O*-dansyl GC (**24**) as well as **23** in a 1:1 ratio.

All compounds were characterized by NMR spectroscopy and high-resolution mass spectrometry (HRMS). Purity of the derivatives **16–24**, with aromatic groups, was determined by high-performance liquid chromatography (HPLC)–UV and ¹H NMR and was in the range of 98–100%. Because ginkgolides (**1–5**) and bilobalide (**6**) absorb only weakly in the UV spectrum, HPLC–UV cannot be used for determination of purity. Instead, observation of the 12-H ¹H NMR signal of **1–6** is a particularly useful way to determine purity, as this signal has distinct and well-separated δ -values for ginkgolides, bilobalide, and their derivatives.

Pharmacology. The native TTLs (**1–6**), as well as ginkgolide derivatives **16–24**, were tested for their ability to bind to PAFR using a radioligand binding assay with membrane fractions from hearts and skeletal muscles of PAFR transgenic mice.⁵³ Initially, compounds were tested in concentrations of 5 μ M against [³H]WEB

Table 1. K_i Values of the Native TTLs


compd	R ₁	R ₂	R ₃	K_i (μM) ^a
GA (1)	H	H	OH	1.46
GB (2)	OH	H	OH	0.56
GC (3)	OH	OH	OH	12.6
GJ (4)	H	OH	OH	9.90
GM (5)	OH	OH	H	>50
bilobalide (6)				>50

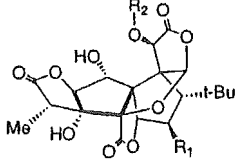
^a Inhibition of [³H]WEB 2086 binding. Values are means of two independent experiments performed in triplicate.

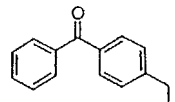
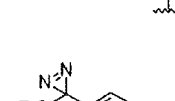
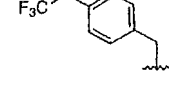
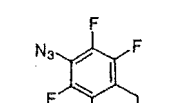
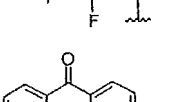
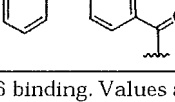
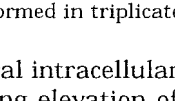
2086 (Figure 2), a potent, competitive PAFR antagonist and [³H]PAF; the compounds were generally less potent against [³H]PAF, but the relative potencies were comparable with the two radioligands. The degree of non-specific binding was determined to be ca. 50% for [³H]PAF and less than 5% for [³H]WEB 2086. Accordingly, the assays were performed using [³H]WEB 2086 rather than [³H]PAF as the radioligand, due to the high degree of nonspecific binding of the latter.

All compounds were dissolved in DMSO to obtain 5 mM stock solutions of test compounds. Examination of the effect of DMSO on the binding of [³H]WEB 2086 revealed that up to 1% DMSO (final concentration) was acceptable, but 1–2.5% resulted in a slight inhibition of [³H]WEB 2086 binding. Generally, this caused no problem; however, with very weakly binding compounds, the relatively high DMSO concentration in solutions above 100 μM had a small inhibitory effect, thus leading to a slight overestimation of their potencies. Previous studies have reported problems associated with the solubilization of ginkgolides specifically in DMSO,⁵⁵ but similar problems were not observed in the present study.

Native ginkgolides (1–5) and bilobalide (6) were tested with the cloned PAFR (Table 1). GB (2) was the most potent compound with a K_i value of 0.56 μM , while GA (1) was slightly less potent with a K_i of 1.46 μM . GC (3) and ginkgolide J (GJ, 4) were significantly less potent, while ginkgolide M (GM, 5) and bilobalide (6) both had K_i values larger than 50 μM .

The GB-derived photoactivatable compounds 16, 18, 20, and 22 with K_i values in the range 0.09–0.15 μM (Table 2) were all more potent than GB (2), while compounds 17, 19, and 21 derived from GC (3) with K_i values of 0.47–0.79 μM were equipotent to GB (2) (Table 2), despite the fact that GC (3) itself is only weakly potent. Besides proving that aromatic groups linked to 10-OH enhance activity in both GB (2) and GC (3) derivatives, these results also indicate that the specific type of photoactivatable group was less important. Derivatives 23 and 24 possessing a fluorescent dansyl group at either 1- or 7-OH were both less potent than 10-*O*-benzophenone GC (17) without the dansyl group, with K_i values of 3.94 and 0.96 μM for 23 and 24, respectively. However, an important difference was observed in the activities between the two; the 1- and 10-disubstituted analogue (24) was ca. four times more potent than the 7- and 10-disubstituted analogue (23).

Table 2. K_i Values of the Synthesized Derivatives


compd	R ₁	R ₂	K_i (μM) ^a
16	H		0.15
17	OH		0.58
18	H		0.15
19	OH		0.47
20	H		0.09
21	OH		0.79
22	H		0.13

^a Inhibition of [³H]WEB 2086 binding. Values are means of two independent experiments performed in triplicate.

PAFR is linked to several intracellular signal transduction pathways including elevation of intracellular calcium concentration,²² which can be used for analyzing functional responses of PAFR ligands.⁵⁶ In the present study, the compounds with K_i values below 5 μM , i.e., GA (1), GB (2), and analogues 16–22, were investigated for their ability to mobilize intracellular calcium in Chinese hamster ovary (CHO) cells expressing the PAFR.⁵⁷ While none of them evoked calcium responses, they all suppressed PAF-induced intracellular calcium increase (data not shown) confirming their function as PAFR antagonists. Because the assay is based on the measurement of the fluorescence of a Ca^{2+} sensitive dye, the fluorescence of analogues 23 and 24 interfered with the measurement and could not be assayed.

Discussion

Nine analogues (16–24) with photoactivatable groups, and in the case of 23 and 24 with fluorescent dansyl groups as well, have been prepared from native ginkgolides GB (2) and GC (3) by selective derivatizations of the hydroxyl groups. Generally, the increased reactivity of the 1-OH and 10-OH as compared to 7-OH has been rationalized by stabilization of the corresponding alkoxides by hydrogen bonding between 1-OH and 10-OH,⁵⁸ but this does not explain the interesting selectivity for the 10-OH position in reactions with benzyl bromide derivatives. Notably, reaction of GC (3) with a bulky silyl chloride protection group occurs exclusively at the 1-OH of GC.⁵⁹ Three different photoactivatable moieties, all of them benzyl derivatives, were incorpo-

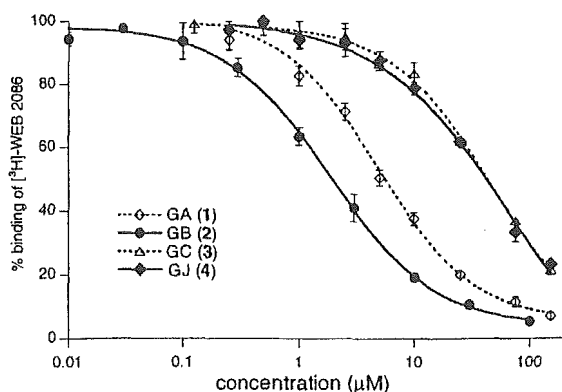


Figure 3. Concentration–displacement curves for native TTLs, as measured by their ability to displace binding of [³H]-WEB 2086 to the cloned PAFR. GB (2) was the most potent analogue, while GA (1) was slightly less potent, and GC (3) and GJ (4) were only weak antagonists. Bars represent the standard deviation (SD).

rated into both GB and GC. The benzophenone moiety was commercially available, whereas trifluoromethyl-diazirine **12** and tetrafluorophenyl azide **15** moieties were synthesized in six and three steps, respectively (Scheme 1). The three different types of photoactivatable groups were selected on the basis of their different reactive intermediates when irradiated, the intermediates being a radical, a carbene, and (singlet) nitrene for benzophenone, trifluoromethyl-diazirine, and tetrafluorophenyl azide, respectively.

All native TTLs (1–6) as well as the derivatized compounds were investigated with respect to their binding to cloned PAFR isolated from transgenic mice (Figure 3 and 4). To the best of our knowledge, this is the first report on the effect of TTLs on the cloned PAFR, since previous SAR studies of PAFR antagonism with TTLs and derivatives was performed by monitoring inhibition of PAF-induced rabbit platelet aggregation. GB (2) has generally been reported to be a potent antagonist of the PAFR based on the latter assay with an IC₅₀ value around 0.2 μM,^{40–42} which corresponds to the K_i value of 0.56 μM obtained in this study (Table 1). GA (1), with one hydroxyl group less than GB (2), was only slightly less potent than GB (2, Figure 3), indicating that the OH-1 is not essential for activity, and neither is the hydrogen bonding between OH-1 and OH-10. Generally, the binding of GC (3), GJ (4), and GM (5) with hydroxyl groups at C-7, as compared to the binding activity of GA (1) and GB (2) lacking the 7-OH, was decreased showing that the 7-OH is not necessary for binding to PAFR whereas hydroxyl groups at other positions appear to be less important (Figure 3). The study also confirmed that bilobalide (6), a TTL with only one five-membered carbocycle and three lactones, is not displacing [³H]WEB 2086 binding in concentrations up to 100 μM (Table 1).

All seven photoactivatable analogues **16–22** with aromatic substituents at 10-OH improved the affinity to the PAFR relative to the activities of GB (2) and GC (3) (Figure 4). This is in agreement with previous SAR studies of GB (2),^{40–42} as well as a three-dimensional (3D)-quantitative SAR (QSAR) study on ginkgolides.⁶⁰ However, it is interesting to note that aromatic substitutions at 10-OH of GC (3) as in compounds **17**, **19**, and **21** improve the affinity to PAFR ca. 20-fold thus making

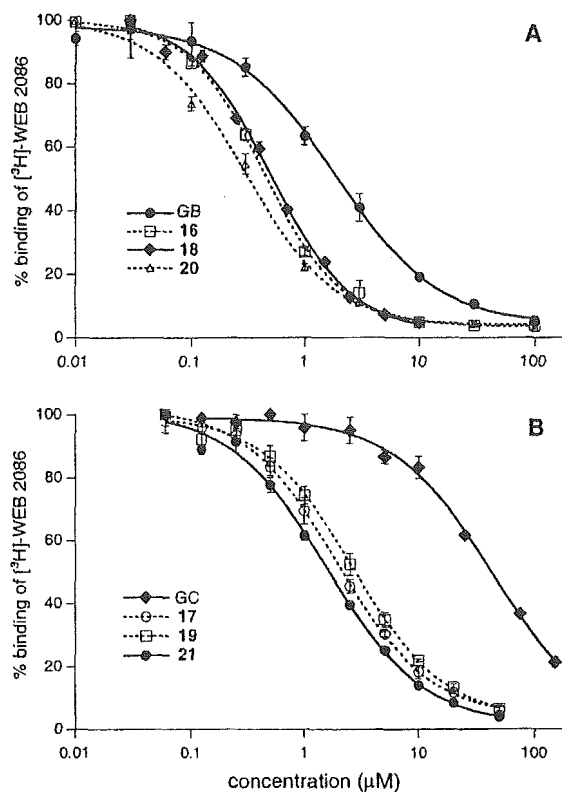


Figure 4. (A) GB (2) and photoactivatable benzyl derivatives; the three photoactivatable derivatives **16**, **18**, and **20** were all ca. 6-fold more potent than GB (2), and the activities were remarkably similar although bearing very different functional groups. (B) GC (3) and photoactivatable benzyl derivatives (**17**, **19**, and **21**) were all more potent than GC (3), with a remarkable increase in potency, thus being equipotent to GB (2). Bars represent the SD.

them equipotent to GB (2), while the same substitutions in GB (2) increase the affinity only 6-fold (Figure 4). Furthermore, the similar affinities of GB derivatives **16**, **18**, **20**, and **22** and the similar affinities of GC derivatives **17**, **19**, and **21** (Figure 4) imply that it is the steric bulk or the lipophilicity, including π - π interactions of the substituents, rather than the specific functional groups that are important for the increase in affinity.

GC derivatives **23** and **24** (Scheme 3) with dansyl groups at 7-OH and 1-OH are less potent and equipotent, respectively, to their parent compound, 10-*O*-benzophenone-GC (**17**). In compound **23**, which is ca. six times less active than **17**, the bulk at the 7-position seems to be responsible for the reduction in affinity. The fact that compound **24** is equipotent to **17** suggests that once a bulky aromatic group occupies this area, further aromatic groups neither increase nor decrease the affinity.

In conclusion, an investigation of the effect of TTLs isolated from *G. biloba* on the cloned PAFR has demonstrated that among the native compounds, GA (1) and GB (2) are the most potent. A series of photoactivatable analogues have been prepared, and PAFR binding assays showed that most of these analogues were more potent antagonists than their parent compounds, thus providing promising candidates for the planned studies of the interaction of ginkgolides with the PAFR. The ginkgolide derivative containing both a photoactivatable and a fluorescent group, compound **24**, retained affinity

to PAFR and thus could be useful in photolabeling and subsequent sequencing studies.

Experimental Section

Chemistry. General Procedures. Ginkgolides and bilobalide (**1–6**) were obtained by extraction of leaves from *G. biloba*, purification by column chromatography, and recrystallization, as previously described,^{3,61} and purity was >99% as determined by ¹H NMR. Solvents were dried by eluting through alumina columns. Triethylamine was freshly distilled from NaOH pellets. Unless otherwise noted, materials were obtained from a commercial supplier and were used without further purification. All reactions were performed in predried glassware under argon or nitrogen, and all reactions involving azides or diazirines were performed in dim red light. Flash column chromatography was performed using ICN silica gel (32–63 mesh) or ICN silica gel (32–63 mesh) impregnated with sodium acetate.⁶¹

Thin-layer chromatography (TLC) was carried out using precoated silica gel 60 F₂₅₄ plates with thickness of 0.25 μm. Spots were observed at 254 nm and by staining with acetic anhydride or cerium/molybdenum in H₂SO₄. ¹H and ¹³C NMR spectra were obtained on Bruker DMX 300 or Bruker DMX 400 MHz spectrometers and are reported in parts per million (ppm) relative to internal solvent signal, with coupling constants (*J*) in Hertz (Hz). For ¹⁹F NMR spectra, hexafluorobenzene (–162.9 ppm) was used as internal standard. Analytical HPLC was performed on a HP 1100 LC instrument using a 5 μm C18 reversed-phase Phenomenex Luna column (150 mm × 4.60 mm), using 1 mL/min of water/acetonitrile/TFA 60:40:0.1, raising to 50:50:0.1 after 10 min, and detecting by UV at 219 and 254 nm. Accurate mass determination was performed on a JEOL JMS-HX110/100A HF mass spectrometer using a 3-nitrobenzyl alcohol (NBA) matrix and Xe ionizing gas, and all are within ±5 ppm of theoretical values.

2,2,2-Trifluoro-1-(4-methylphenyl)-1-ethanone (7).⁴⁸ 4-Bromotoluene (9.45 g, 55.25 mmol) was dissolved in Et₂O (280 mL) and cooled to –40 °C. *n*-Butyllithium (1.1 M in hexane, 40.5 mL, 60.74 mmol) was added dropwise, and the solution was warmed to 0 °C over a 2 h period. The solution was then cooled to –60 °C and a solution of *N*-trifluoroacetylperidine⁴⁸ (10.00 g 55.23 mmol) in dry Et₂O (60 mL) was added in portions. The reaction was allowed to stir at –60 °C for 3 h and then warmed to room temperature. The solution was hydrolyzed with saturated NH₄Cl (50 mL) and washed with NH₄Cl (5 × 50 mL) and H₂O (3 × 50 mL). The organic phase was dried (MgSO₄), and the solvent was removed in vacuo. The remaining oil was purified by flash column chromatography eluting with hexane/CH₂Cl₂ (5:1, 4:1, and 3:1) to give a colorless oil (5.62 g, 54%). ¹H NMR (300 MHz, CDCl₃): δ 2.46 (s, 3H), 7.26–7.36 and 7.96–7.98 (AA'BB' system, 4H). ¹³C NMR (75 MHz, CDCl₃): δ 22.3, 117.0 (q, ¹J_{CF} = 292.5, CF₃), 127.9, 130.2 (2 C), 130.7 (2 C), 147.4, 169.1 (q, ²J_{CF} = 60.0).

2,2,2-Trifluoro-1-(4-methylphenyl)-1-ethanone Oxime (8).⁴⁸ Ketone **7** (2.60 g, 13.80 mmol) was dissolved in pyridine (30 mL), hydroxylamine hydrochloride (2.88 g, 41.44 mmol) was added, and the reaction was stirred at 70 °C for 3 h. Pyridine was removed in vacuo, and the remaining residue was dissolved in Et₂O (50 mL) and washed with 0.01 M HCl (50 mL). The organic layer was washed with H₂O (3 × 50 mL) and dried (MgSO₄), and the solvent was removed in vacuo to give a colorless solid (2.01 g, 72%), which was used without further purification. ¹H NMR (300 MHz, CDCl₃): δ 2.40 (s, 3H), 7.20–7.30 and 7.37–7.43 (m, 4H), 8.38 (bs, OH). Multiple splitting patterns arise due to anti/syn configurations of the oxime. ¹³C NMR (75 MHz, CDCl₃): δ 21.9, 121.0 (q, ¹J_{CF} = 277.5, CF₃), 123.4, 129.0 (2C), 129.7 (2C), 141.4, 148.4 (q, ²J_{CF} = 37.5).

2,2,2-Trifluoro-1-(4-methylphenyl)-1-ethanone *O*-(*p*-Toluenesulfonyl) Oxime (9).⁴⁸ To a stirred solution of oxime **8** (2.00 g, 9.85 mmol) in pyridine (36 mL), *p*-toluenesulfonyl chloride (2.82 g, 14.79 mmol) was added in portions and the reaction mixture was refluxed for 3 h. Pyridine was removed in vacuo, and the residue was purified by flash column

chromatography eluting with hexane/CH₂Cl₂ (2:1) to give a white solid (2.90 g, 82%). ¹H NMR (300 MHz, CDCl₃): δ 2.40 (s, 3H), 2.48 (s, 3H), 7.26–7.34 (m, 4H), 7.37–7.40 and 7.87–7.90 (AA'BB' system, tosyl aromatic H, 4H). ¹³C NMR (75 MHz, CDCl₃): δ 21.9, 22.2, 120.0 (q, ¹J_{CF} = 285.0, CF₃), 122.0, 128.9 (2C), 129.7 (2C), 129.9 (2C), 130.2 (2C), 132.0, 142.7, 146.4, 154.0 (q, ²J_{CF} = 67.5).

3-(4-Methylphenyl)-3-trifluoromethyldiaziridine (10).⁴⁸ In a thick-walled screw-cap tube, **9** (2.90 g, 8.12 mmol) was dissolved in Et₂O (20 mL). The solution was cooled to –78 °C, and liquid ammonia (3.5 mL) was added. The tube was screwed tightly, and the solution allowed rising to room temperature. The reaction was stirred for 12 h, and the solution was cooled to –78 °C. The cap was removed, and the mixture risen to room temperature to remove ammonia. The solution was partitioned between Et₂O (50 mL) and H₂O (50 mL), the organic layer was dried (MgSO₄), and the solvent was removed in vacuo. The product was purified by flash column chromatography eluting with chloroform to give a colorless solid (1.25 g, 77%). ¹H NMR (300 MHz, CDCl₃): δ 2.19 (NH, d, 1H), 2.38 (s, 3H), 2.74 (NH, d, 2H), 7.22–7.24 and 7.49–7.51 (AA'BB' system, 4H). ¹³C NMR (75 MHz, CDCl₃): δ 21.7, 57.9 (q, ²J_{CF} = 34.9), 125.0 (q, ¹J_{CF} = 278.7, CF₃), 129.3 (2C), 129.7 (2C), 130.1, 140.0.

3-(4-Methylphenyl)-3-trifluoromethyldiazirine (11).⁴⁸ Diaziridine **10** (1.25 g, 6.18 mmol) was dissolved in CH₂Cl₂ (25 mL), and triethylamine (2.58 mL, 18.54 mmol) was added and cooled to 0 °C. Iodine (1.73 g, 6.80 mmol) was added in small portions until a brown color persisted. The solution was washed with 1 M NaOH (25 mL), H₂O (25 mL), and brine (25 mL). The organic phase was dried (MgSO₄), and the solvent was carefully removed in vacuo at 20 °C due to volatility of the product. The crude product was purified by flash column chromatography eluting with hexane/CH₂Cl₂ (20:1) to give a colorless solid (1.03 g, 82%). ¹H NMR (300 MHz, CDCl₃): δ 2.36 (s, 3H), 7.07–7.10, 7.19 and 7.22 (AA'BB' system, 4H). ¹³C NMR (100 MHz, CDCl₃): δ 21.5, 28.9 (q, ²J_{CF} = 39.6), 123.0 (q, ¹J_{CF} = 274.7, CF₃), 125.5, 127.1 (2C), 130.8 (2C), 141.1.

3-(4-Bromomethylphenyl)-3-trifluoromethyldiazirine (12).⁴⁹ A solution of diazirine **11** (0.50 g, 2.50 mmol) in CCl₄ (10 mL) was heated to 70 °C and powdered NBS (0.66 g, 3.75 mmol) was added and stirred for 10 min, then AIBN (10 mg) was added, and the reaction was refluxed for 2 h. The precipitate was filtered, the solvent was removed in vacuo at 20 °C, and the crude product was purified by column chromatography eluting with hexane/CH₂Cl₂ (20:1) to give an oil (0.30 g, 40%). ¹H NMR (400 MHz, CDCl₃): δ 4.50 (s, 2H), 7.17–7.23, 7.43 and 7.47 (AA'BB' system, 4H). ¹³C NMR (100 MHz, CDCl₃): δ 28.3 (q, ²J_{CF} = 40.5), 39.7, 122.2 (q, ¹J_{CF} = 275.0, CF₃), 127.3 (2C), 129.6, 129.9 (2C), 139.8.

4-Azidotetrafluorobenzaldehyde (13).⁵⁰ To a solution of pentafluorobenzaldehyde (2.69 g, 13.72 mmol) in acetone (24 mL) and H₂O (9 mL), NaN₃ (1.06 g, 14.54 mmol) was added and the mixture was refluxed for 8 h. The solution was cooled to room temperature and diluted with H₂O (20 mL). The solution was extracted with ether (3 × 30 mL), the organic phase was dried (MgSO₄), and the solvent was removed in vacuo. The maroon-colored gum was sublimed at 70 °C under reduced pressure to give a colorless solid (1.80 g, 60%). ¹⁹F NMR (282 MHz, CDCl₃): δ –152.14 (m, 2F), –146.10 (m, 2F).

4-Azidotetrafluorobenzyl Alcohol (14).⁵⁰ 4-Azidotetrafluorobenzaldehyde (**13**, 1.80, 8.21 mmol) was dissolved in acetic acid (27 mL), and Me₂NH·BH₃ (0.58 g, 9.85 mmol) was added. The reaction was stirred at room temperature for 1 h. The acid versatiles were removed in vacuo at 45 °C. The residue was dissolved in CHCl₃ (10 mL) and washed with 5% Na₂CO₃ (3 × 10 mL). The organic phase was dried (MgSO₄), and the solvent was removed in vacuo to give a colorless solid (1.74 g, 97%), which was used without further purification. ¹H NMR (300 MHz, CDCl₃): δ 2.41 (OH, broad s, 1H), 4.79 (s, 2H). ¹⁹F NMR (282 MHz, CDCl₃): δ –150.90 (m, 2F), –143.75 (m, 2F).

1-Azido-4-(bromomethyl)-2,3,5,6-tetrafluorobenzene (15).^{51,52} Alcohol **14** (1.74 g, 7.93 mmol) was dissolved in a

mixture of CHCl_3 (40 mL) and pyridine (0.32 mL, 3.97 mmol). Three portions of PBr_3 (3×0.05 mL, 1.58 mmol) were added dropwise every 30 min to the refluxing solution. After the last portion of PBr_3 was added, the reaction was refluxed for 2 h. The solution was cooled to room temperature, 2-propanol (20 mL) was added, and the reaction was stirred for an additional 10 min. The solution was washed with 1 N NaHCO_3 (3×50 mL) and dried (MgSO_4), and the solvent was removed in vacuo to give a white solid. The crude product was purified by flash column chromatography eluting with hexane/ethyl acetate (8:1) to give a slightly yellow solid (1.20 g, 53%). ^1H NMR (300 MHz, CDCl_3): δ 4.51 (s, 2H). ^{19}F NMR (282 MHz, CDCl_3): δ -150.50 (m, 2F), -141.80 (m, 2F).

Synthesis of 16–21. General Synthetic Procedure. GB (2) or GC (3) (0.07 mmol) was dissolved in THF (4 mL), and KH (0.008 g, 0.24 mmol) was added at room temperature. The reaction mixture was stirred for 10 min, and then, a solution of 4-(bromomethyl)benzophenone, **12**, or **15** (0.212 mmol) in THF (1 mL) was added dropwise. The reaction was stirred at room temperature for 4 h. The solution was then cooled to 0 °C, and concentrated HCl (0.3 mL) was added. The mixture was diluted with H_2O (10 mL), extracted with EtOAc (3×10 mL), and washed with saturated aqueous NH_4Cl solution (30 mL), brine (30 mL), and H_2O (30 mL). The organic phase was dried (MgSO_4), and the solvent was removed in vacuo. The crude material was purified by flash column chromatography using either A: $\text{CHCl}_3/\text{MeOH}$ (100:1 and 50:1), B: $\text{CHCl}_3/\text{MeOH}$ (30:1 and 20:1), or C: cyclohexane/acetone (3:1 and 2:1). All ginkgolide derivatives were white solids that decomposed above 250 °C.

10-O-Benzophenone Ginkgolide B (16). Purified by method B; yield, 0.035 g (78%). ^1H NMR (400 MHz, CD_3OD): δ 1.13 (s, *tert*-butyl), 1.24 (d, $J = 7.1$, CH_3), 1.92 (dd, $J = 14.3$, 4.5, 8-H), 2.07 (td, $J = 13.9$, 4.4, 7 α -H), 2.27 (dd, $J = 13.5$, 4.6, 7 β -H), 3.06 (q, $J = 7.1$, 14-H), 4.31 (d, $J = 7.2$, 1-H), 4.55 (d, $J = 7.2$, 2-H), 4.85 (d, $J = 11.5$, benzylic-H, 1H), 5.28 (s, 10-H), 5.42 (d, $J = 4.0$, 6-H), 5.59 (d, $J = 11.5$, benzylic-H, 1H), 6.15 (s, 12-H), 7.53–7.60 (m, Ar-H, 4H), 7.65–7.67 (m, Ar-H, 1H), 7.77–7.82 (m, Ar-H, 4H). ^{13}C NMR (100 MHz, CD_3OD): δ 7.25, 28.46 (3C), 32.18, 37.26, 42.29, 49.61, 68.21, 72.59, 72.80, 74.45, 76.76, 79.48, 83.53, 93.15, 99.78, 110.83, 127.96 (2C), 128.58 (2C), 130.03 (2C), 130.52 (2C), 132.94, 137.76 (2C), 141.67, 171.52, 172.70, 177.33, 196.45. HPLC–UV: 98.5%. HRMS: $\text{C}_{34}\text{H}_{34}\text{O}_{11}$ requires $M + \text{Na}$ at m/z 641.1999; found, 641.2018.

10-O-Benzophenone Ginkgolide C (17). Purified by method A; yield, 0.023 g (64%). ^1H NMR (400 MHz, CD_3OD): δ 1.20 (s, *tert*-butyl), 1.24 (d, $J = 7.1$, CH_3), 1.78 (d, $J = 12.5$, 8-H), 3.04 (q, $J = 7.1$, 14-H), 4.21 (dd, $J = 12.5$, 4.3, 7-H), 4.28 (d, $J = 7.0$, 1-H), 4.54 (d, $J = 7.0$, 2-H), 4.87 (d, $J = 11.6$, benzylic-H, 1H), 5.13 (d, $J = 4.3$, 6-H), 5.28 (s, 10-H), 5.60 (d, $J = 11.6$, benzylic-H, 1H), 6.17 (s, 12-H) 7.53–7.61 (m, Ar-H, 4H), 7.65–7.67 (m, Ar-H, 1H), 7.77–7.83 (m, Ar-H, 4H). ^{13}C NMR (100 MHz, CD_3OD): δ 7.34, 28.50 (3C), 32.12, 42.26, 50.00, 64.48, 67.40, 72.77, 74.28, 75.14, 76.74, 79.49, 83.55, 93.28, 99.54, 110.63, 127.95 (2C), 128.59 (2C), 130.03 (2C), 130.53 (2C), 132.96, 137.68 (2C), 141.65, 171.41, 172.55, 177.27, 197.03. HPLC–UV: 99.3%. HRMS: $\text{C}_{34}\text{H}_{34}\text{O}_{12}$ requires $M + 1$ at m/z 635.2129; found, 635.2098.

10-O-(Trifluoromethyl-3H-diazirine)benzyl Ginkgolide B (18). Purified by method B; yield, 0.024 g (59%). ^1H NMR (400 MHz, CD_3OD): δ 1.11 (s, *tert*-butyl), 1.23 (d, $J = 7.1$, CH_3), 1.89 (dd, $J = 14.3$, 4.3, 8-H), 2.01 (td, $J = 13.9$, 4.3, 7 α -H), 2.25 (dd, $J = 13.4$, 4.4, 7 β -H), 3.05 (q, $J = 7.1$, 14-H), 4.27 (d, $J = 7.3$, 1-H), 4.53 (d, $J = 7.3$, 2-H), 4.77 (d, $J = 11.2$, benzylic-H, 1H), 5.24 (s, 10-H), 5.39 (d, $J = 3.9$, 6-H), 5.51 (d, $J = 11.2$, benzylic-H, 1H), 6.14 (s, 12-H), 7.29 and 7.53 (AA'BB' system, Ar-H, 4H). ^{13}C NMR (75 MHz, CDCl_3): δ 7.67, 21.57 (q, $^2J_{\text{CF}} = 40.9$, CCF_3), 29.56 (3C), 32.65, 37.49, 49.31, 68.07, 72.88, 73.57, 74.57, 76.56, 77.65, 80.08, 83.90, 90.90, 99.05, 110.68, 122.33 (q, $^1J_{\text{CF}} = 274.3$, CF_3), 127.83 (2C), 129.53 (2C), 131.06, 136.44, 171.25, 171.50, 175.87. ^{19}F NMR (282 MHz, CDCl_3): δ -66.23 (s, 3F). HPLC–UV: 99.1%. HRMS: $\text{C}_{29}\text{H}_{29}\text{F}_3\text{N}_2\text{O}_{10}$ requires $M + 1$ at m/z 623.1853; found, 623.1834.

10-O-(Trifluoromethyl-3H-diazirine)benzyl Ginkgolide C (19). Purified by method A; yield, 0.023 g (51%). ^1H NMR (400 MHz, CD_3OD): δ 1.17 (s, *tert*-butyl), 1.24 (d, $J = 7.1$, CH_3), 1.76 (d, $J = 12.5$, 8-H), 3.02 (q, $J = 7.1$, 14-H), 4.15 (dd, $J = 12.5$, 4.3, 7-H) 4.24 (d, $J = 7.0$, 1-H), 4.52 (d, $J = 7.0$, 2-H), 4.79 (d, $J = 11.3$, benzylic-H, 1H), 5.10 (d, $J = 4.3$, 6-H), 5.23 (s, 10-H), 5.52 (d, $J = 11.3$, benzylic-H, 1H), 6.15 (s, 12-H), 7.29 and 7.54 (AA'BB' system, aromatic-H, 4H). ^{13}C NMR (75 MHz, CDCl_3): δ 7.65, 23.77 (q, $^2J_{\text{CF}} = 38.9$, CCF_3), 29.52 (3C), 32.65, 41.94, 50.92, 64.43, 67.48, 73.89, 74.30, 76.03, 76.34, 79.63, 83.90, 90.91, 98.94, 110.53, 122.32 (q, $^1J_{\text{CF}} = 275.0$, CF_3), 127.94 (2C), 129.68 (2C), 131.26, 136.07, 170.97, 171.07, 175.69. ^{19}F NMR (282 MHz, CDCl_3): δ -66.25 (s, 3F). HPLC–UV: 97.9%. HRMS: $\text{C}_{29}\text{H}_{29}\text{F}_3\text{N}_2\text{O}_{11}$ requires $M + 1$ at m/z 639.1802; found, 639.1790.

10-O-Tetrafluorobenzyl Azide Ginkgolide B (20). Purified by method B; yield, 0.023 g (50%). ^1H NMR (400 MHz, CDCl_3): δ 1.13 (s, *tert*-butyl), 1.32 (d, $J = 7.0$, CH_3), 1.84–1.97 (m, 8-H and 7 α -H), 2.27–2.33 (m, 7 β -H), 2.84 (d, $J = 3.5$, 1-OH), 2.99 (s, 3-OH), 3.06 (q, $J = 7.0$, 14-H), 4.29 (dd, $J = 7.9$, 3.5, 1-H), 4.61 (d, $J = 7.9$, 2-H), 4.81 (d, $J = 10.7$, benzylic-H, 1H), 4.94 (s, 10-H), 5.39 (d, $J = 3.4$, 6-H), 5.64 (d, $J = 10.7$, benzylic-H, 1H), 6.03 (s, 12-H). ^{13}C NMR (100 MHz, CDCl_3): δ 7.70, 29.52 (3C), 32.62, 37.37, 42.03, 49.30, 61.21, 68.11, 72.79, 74.65, 80.07, 83.89, 91.00, 99.12, 108.95, 110.73, 139.71, 142.24, 144.45, 147.10, 170.69, 171.45, 175.83. ^{19}F NMR (282 MHz, CDCl_3): δ -143.31 (m, 2F), -150.85 (m, 2F). HPLC–UV: 98.8%. HRMS: $\text{C}_{27}\text{H}_{25}\text{F}_4\text{N}_3\text{O}_{10}$ requires $M + 1$ at m/z 628.1554; found, 628.1565.

10-O-Tetrafluorobenzyl Azide Ginkgolide C (21). Purified by method C; yield, 0.080 g (54%). ^1H NMR (400 MHz, CDCl_3): δ 1.22 (s, *tert*-butyl), 1.33 (d, $J = 7.0$, CH_3), 1.71 (d, $J = 12.4$, 8-H), 2.33 (d, $J = 10.6$, 7-OH), 2.88 (d, $J = 3.4$, 1-OH), 3.01 (s, 3-OH), 3.08 (q, $J = 7.0$, 14-H), 4.08 (m, 7-H) 4.27 (dd, $J = 7.8$, 3.4, 1-H), 4.62 (d, $J = 7.8$, 2-H), 4.83 (d, $J = 10.7$, benzylic-H, 1H), 4.96 (s, 10-H), 5.09 (d, $J = 4.4$, 6-H), 5.58 (d, $J = 10.7$, benzylic-H, 1H), 6.04 (s, 12-H). ^{13}C NMR (75 MHz, CDCl_3): δ 7.64, 29.42 (3C), 32.59, 42.08, 50.64, 51.16, 61.47, 64.35, 67.32, 74.27, 75.88, 79.64, 83.88, 91.26, 99.14, 110.71, 120–150 (m, 6C), 170.72, 171.17, 176.29. ^{19}F NMR (282 MHz, CDCl_3): δ -143.56 (m, 2F), -151.08 (m, 2F). HPLC–UV: 99.1%. HRMS: $\text{C}_{27}\text{H}_{25}\text{F}_4\text{N}_3\text{O}_{11}$ requires $M + 1$ at m/z 644.1503; found, 644.1527.

10-O-Benzoylbenzoic Ginkgolide C (22). 4-Benzoylbenzoic acid (0.018 g, 0.08 mmol) and **2** (0.028 g, 0.07 mmol) were dissolved in THF (5 mL), and the mixture was cooled to 0 °C. EDC (0.018 g, 0.092 mmol) and DMAP (0.002 g, 0.01 mmol) were added, and the reaction mixture was stirred at 0 °C for 1 h and continued overnight at room temperature. The solvent was removed in vacuo, and the crude product was dissolved in EtOAc (20 mL) and washed with a saturated 5% NaHCO_3 solution (20 mL) and brine (20 mL). The organic fraction was dried (MgSO_4), and the solvent was evaporated in vacuo. The crude product was purified by flash column chromatography eluting with hexane/EtOAc (2:1) to give the product as white crystals (0.026 g, 62%). ^1H NMR (400 MHz, CD_3OD): δ 1.07 (s, *tert*-butyl), 1.26 (d, $J = 7.1$, CH_3), 1.98–2.10 (m, 8-H and 7 α -H), 2.30–2.36 (m, 7 β -H), 3.12 (q, $J = 7.1$, 14-H), 4.37 (d, $J = 6.5$, 1-H), 4.55 (d, $J = 6.5$, 2-H), 5.66 (d, $J = 3.2$, 6-H), 6.32 (s, 10-H), 6.45 (s, 12-H), 7.54–7.58 (m, Ar-H, 2H), 7.67–7.69 (m, Ar-H, 1H), 7.80–7.83 (m, Ar-H, 2H), 7.86–7.88 (m, Ar-H, 2H), 8.42–8.44 (m, Ar-H, 2H). ^{13}C NMR (100 MHz, CD_3OD): δ 7.42, 28.22 (3C), 32.16, 37.27, 42.29, 49.42, 67.81, 70.64, 72.74, 74.42, 79.29, 83.64, 95.13, 100.51, 111.12, 128.73 (2C), 129.92 (2C), 130.17 (2C), 130.58 (2C), 131.61, 133.41, 137.06, 142.66, 164.56, 168.93, 171.41, 177.33, 196.48. HPLC–UV: 99.2%. HRMS: $\text{C}_{34}\text{H}_{31}\text{O}_{12}$ requires $M + \text{Na}$ at m/z 655.1791; found, 655.1790.

10-O-Benzophenone-7-O-dansyl Ginkgolide C (23). A solution of dansyl chloride (0.010 g, 0.035 mmol) in acetonitrile (0.3 mL) was added to a solution of **17** (0.020 g, 0.032 mmol) and DMAP (0.008 g, 0.063 mmol) in acetonitrile (1.5 mL). The reaction mixture was stirred for 16 h at room temperature, then a saturated aqueous NH_4Cl solution (2 mL) was added,

and the mixture was extracted with EtOAc (3 × 5 mL). The combined organic phase was washed with saturated aqueous NaCl solution (3 × 15 mL), dried (MgSO₄), and the solvent was removed in vacuo. The crude product was purified by flash column chromatography eluting with cyclohexane/acetone (2:1) to give the product as a slightly yellow solid (0.015 g, 56%). ¹H NMR (400 MHz, DMSO-*d*₆): δ 0.83 (s, *tert*-butyl), 1.09 (d, *J* = 7.2, CH₃), 1.94 (d, *J* = 12.5, 8-H), 2.81 [m, 14-H and N(CH₃)₂], 4.26 (t, *J* = 5.3, 1-H), 4.53 (d, *J* = 5.4, 2-H), 4.79 (d, *J* = 13.2, benzylic-H, 1H), 4.89 (dd, *J* = 12.5, 4.0, 7-H), 5.19 (d, *J* = 4.0, 6-H), 5.23 (s, 10-H), 5.46 (d, *J* = 13.2, benzylic-H, 1H), 6.07 (d, *J* = 5.3, 1-OH), 6.21 (s, 12-H), 6.51 (s, 3-OH), 7.28–7.30 (m, Ar–H, 1H), 7.50–7.70 (m, Ar–H, 7H), 7.79–7.82 (m, Ar–H, 4H), 8.18–8.20 (m, Ar–H, 2H), 8.54–8.56 (m, Ar–H, 1H). HPLC–UV: 98.9%. HRMS: C₄₆H₄₅NO₁₄S requires *M* + 1 at *m/z* 868.2639; found, 868.2642.

10-*O*-benzophenone-1-*O*-dansyl Ginkgolide C (24). Synthesized as **23** but using 2 equiv of dansyl chloride (instead of 1.1 equiv) gave rise to a ca. 1:1 mixture of **23** and **24**. The two products were separated on analytical TLC giving **24** (0.008 g, 30%) as a slightly yellow solid. ¹H NMR (400 MHz, DMSO-*d*₆): δ 0.91 (s, *tert*-butyl), 1.16 (d, *J* = 7.6, CH₃), 1.78 (d, *J* = 12.5, 8-H), 2.80 [s, N(CH₃)₂], 2.97 (q, *J* = 7.6, 14-H), 4.22 (d, *J* = 3.8, 1-H), 4.26 (m, 7-H), 4.57 (d, *J* = 3.9, 6-H), 4.80 (d, *J* = 13.2, benzylic-H, 1H), 5.20 (d, *J* = 3.8, 2-H), 5.30 (s, 10-H), 5.31 (d, *J* = 4.9, 7-OH), 5.49 (d, *J* = 13.2, benzylic-H, 1H), 5.95 (s, 12-H), 5.98 (s, 3-OH), 7.25–7.27 (m, Ar–H, 1H), 7.54–7.79 (m, Ar–H, 11H), 8.18–8.24 (m, Ar–H, 2H), 8.47–8.49 (m, Ar–H, 1H). HPLC–UV: 99.0%. HRMS: C₄₆H₄₅NO₁₄S requires *M* + 1 at *m/z* 868.2639; found, 868.2668.

Radioligand Binding Assay. Heart and skeletal muscles from 13 to 27 months old PAFR transgenic (PAFR-Tg) mice,⁶² which overexpress guinea pig PAFR, were homogenized in a Polytron homogenizer in cold buffer A [25 mM Hepes/NaOH (pH 7.4), 0.25 M sucrose, 10 mM MgCl₂, 1 mM PMSF, and a protease inhibitor cocktail Complete (Boehringer Mannheim)]. An 800g (for 10 min) supernatant of the homogenate was centrifuged at 100 000g at 4 °C for 1 h, and the resulting pellet was suspended in buffer A and stored at –80 °C until use. The protein concentration of the suspended membrane fraction was 1.37 mg/mL, as measured by the method of Bradford⁶³ using the Bio-Rad protein assay solution and fatty acid-free bovine serum albumin (BSA; Bayer, Kankakee, IL) as a standard. The radioligand binding assays were performed essentially as previously described.⁵³ The membrane fractions from hearts and skeletal muscles of PAFR-Tg mice (50 μL of suspension containing 121 fmol of PAFR) were mixed with 2 pmol of [³H]WEB 2086 (NEN Life Science Products, Boston, MA) in 50 μL of buffer B [25 mM Hepes/NaOH (pH 7.4), 0.25 M sucrose, 10 mM MgCl₂, 0.1% BSA], and the compound was to be tested in 100 μL of buffer B in a 96 well microplate in triplicate for each concentration. These mixtures were incubated at 25 °C for 90 min, upon which the receptor-bound [³H]-WEB 2086 was filtered on a UniFilter-GF/C (Packard Bioscience, Meriden, CT) using a MicroMate 196 simultaneous 96 well harvester (Packard Bioscience). The filter was then washed 10 times with cold buffer B and dried at 50 °C for at least 90 min, 25 μL of MicroScint-0 scintillation cocktail (Packard Bioscience) was added, and filters were placed in a TopCount microplate scintillation counter (Packard Bioscience). Binding data were analyzed with the nonlinear curve-fitting program Microplate Manager III (Bio-Rad, Hercules, CA). Calculated IC₅₀ values were then converted to K_i values using the Cheng–Prusoff correction,⁶⁴ with the following equation: K_i = IC₅₀/(1 + [L]/K_D), where [L] is the concentration of the radioligand, and K_D is the previously determined dissociation constant for [³H]WEB 2086 (4.3 nM).⁵³ Nonspecific binding was determined using methods as previously described.⁵³

Intracellular Calcium Mobilization. CHO cells expressing human PAFR⁵⁷ were subjected to the calcium assay as described previously⁵⁶ except that Fura-2/AM was loaded in the presence of chromophore EL (0.01%, Sigma). Each com-

pound (100 μM) was applied to the cell suspension, and then, PAF (10 nM) was added after 3 min.

Acknowledgment. We are grateful to Dr. Yasuhiro Itagaki for performing HRMS. We thank the Alfred Benzon Foundation (to K.S.) and the NSF REU program (CHE 9820490, to D.R.S., Beloit College, Beloit, WI) for financial support.

References

- (1) Drieu, K.; Jaggy, H. History, development and constituents of EGb 761. In *Medicinal and Aromatic Plants-Industrial Profiles: Ginkgo biloba*; van Beek, T. A., Ed.; Harwood Academic Publishers: Amsterdam, 2000; Vol. 12, pp 267–277.
- (2) Hasler, A. Chemical constituents of Ginkgo biloba. In *Medicinal and Aromatic Plants-Industrial Profiles: Ginkgo biloba*; van Beek, T. A., Ed.; Harwood Academic Publishers: Amsterdam, 2000; Vol. 12, pp 109–142.
- (3) Nakanishi, K. The ginkgolides. *Pure Appl. Chem.* **1967**, *14*, 89–113 and references therein.
- (4) Okabe, K.; Yamada, K.; Yamamura, S.; Takada, S. Ginkgolides. *J. Chem. Soc. C* **1967**, 2201–2206.
- (5) Nakanishi, K.; Habaguchi, K.; Nakadaira, Y.; Woods, M. C.; Maruyama, M.; Major, R. T.; Alauddin, M.; Patel, A. R.; Weinges, K.; Bähr, W. Structure of bilobalide, a rare *tert*-butyl containing sesquiterpenoid related to the C₂₀-ginkgolides. *J. Am. Chem. Soc.* **1971**, *93*, 3544–3546.
- (6) Weinges, K.; Hepp, M.; Jaggy, H. Chemie der Ginkgolide. II. Isolierung und Strukturaufklärung eines neuen Ginkgolids. *Liebigs Ann. Chem.* **1987**, 521–526.
- (7) DeFeudis, F. V.; Drieu, K. Ginkgo biloba extract (EGb 761) and CNS functions: basic studies and clinical applications. *Curr. Drug Targets* **2000**, *1*, 25–58.
- (8) Logani, S.; Chen, M. C.; Tran, T.; Le, T.; Raffa, R. B. Actions of Ginkgo biloba related to potential utility for the treatment of conditions involving cerebral hypoxia. *Life Sci.* **2000**, *67*, 1389–1396.
- (9) Oken, B. S.; Storzbach, D. M.; Kaye, J. A. The efficacy of Ginkgo biloba on cognitive function in alzheimer disease. *Arch. Neurol.* **1998**, *55*, 1409–1415.
- (10) Kleijnen, J.; Knipschild, P. Ginkgo biloba. *Lancet* **1992**, *340*, 1136–1139.
- (11) Söholm, B. Clinical improvement of memory and other cognitive functions by Ginkgo biloba: review of relevant literature. *Adv. Nat. Ther.* **1998**, *15*, 54–65.
- (12) Diamond, B. J.; Shiflett, S. C.; Feiwei, N.; Mathies, R. J.; Noskin, O.; Richards, J. A.; Schoenberger, N. E. Ginkgo biloba extract: mechanisms and clinical indications. *Arch. Phys. Med. Rehabil.* **2000**, *81*, 668–678.
- (13) van Dongen, M. C. J. M.; van Rossum, E.; Knipschild, P. Efficacy of Ginkgo biloba special extracts – evidence from randomized clinical trials. In *Medicinal and Aromatic Plants-Industrial Profiles: Ginkgo biloba*; van Beek, T. A., Ed.; Harwood Academic Publishers: Amsterdam, 2000; Vol. 12, pp 385–442.
- (14) Le Bars, P. L.; Katz, M. M.; Berman, N.; Itil, T. M.; Freedman, A. M.; Schatzberg, A. F. A placebo-controlled double-blind, randomized trial of an extract of Ginkgo biloba for dementia. North American EGb study group. *J. Am. Med. Assoc.* **1997**, *278*, 1327–1332.
- (15) Kanowski, S.; Hermann, W. M.; Stephan, K.; Wierich, W.; Horr, R. Proof of efficacy of Ginkgo biloba special extract EGb 761 in outpatients suffering from mild to moderate primary degenerative dementia of the Alzheimer type or multi-infarct dementia. *Pharmacopsychiatry* **1996**, *29*, 47–56.
- (16) Watanabe, M. H.; Wolfram, S.; Ader, P.; Rimbach, G.; Packer, L.; Maguire, J. J.; Schultz, P. G.; Gohil, K. The in vivo neuromodulatory effects of the herbal medicine Ginkgo biloba. *Proc. Natl. Acad. Sci. U.S.A.* **2001**, *98*, 6577–6580.
- (17) Kennedy, D. O.; Scholey, A. B.; Wesnes, K. A. The dose-dependent cognitive effects of acute administration of Ginkgo biloba to healthy young volunteers. *Psychopharmacology* **2000**, *151*, 416–423.
- (18) Polich, J.; Gloria, R. Cognitive effects of a Ginkgo biloba/vinpocetine compound in normal adults: systematic assessment of perception, attention and memory. *Hum. Psychopharmacol. Clin. Exp.* **2001**, *16*, 409–416.
- (19) Rigney, U.; Kimber, S.; Hindmarch, I. The effects of acute doses of standardized Ginkgo biloba extract on memory and psychomotor performances in volunteers. *Phytother. Res.* **1999**, *13*, 408–415.
- (20) Stough, C.; Clarke, J.; Lloyd, J.; Nathan, P. J. Neuropsychological changes after 30-day Ginkgo biloba administration in healthy patients. *Int. J. Neuropsychopharmacol.* **2001**, *4*, 131–134.

- (21) Braquet, P.; Spinnewyn, B.; Braquet, M.; Bourgain, R. H.; Taylor, J. E.; Etienne, A.; Drieu, K. BN 52021 and related compounds: a new series of highly specific PAF-acether antagonists isolated from *Ginkgo biloba* L. *Blood Vessels* **1985**, *16*, 559–572.
- (22) Ishii, S.; Shimizu, T. Platelet-activating factor (PAF) receptor and genetically engineered PAF receptor mutant mice. *Prog. Lipid Res.* **2000**, *39*, 41–82.
- (23) Prescott, S. M.; Zimmerman, G. A.; Stafforini, D. M.; McIntyre, T. M. Platelet-activating factor and related lipid mediators. *Annu. Rev. Biochem.* **2000**, *69*, 419–445.
- (24) Shukla, S. D. Platelet activating factor. *Biomembranes* **1996**, *2B*, 463–479.
- (25) Bito, H.; Nakamura, M.; Honda, Z.; Izumi, T.; Iwatsubo, T.; Seyama, Y.; Ogura, Y.; Shimizu, T. Platelet-activating factor (PAF) receptor in rat brain: PAF mobilizes intracellular Ca^{2+} in hippocampal neurons. *Neuron* **1992**, *9*, 285–294.
- (26) Mori, M.; Aihara, M.; Kume, K.; Hamanoue, M.; Kohsaka, S.; Shimizu, T. Predominant expression of platelet-activating factor receptor in the rat brain microglia. *J. Neurosci.* **1996**, *16*, 3590–3600.
- (27) Kroegel, C.; Kortsik, C.; Kroegel, N.; Matthys, H. The pathophysiological role and therapeutic implications of platelet-activating factor in diseases of aging. *Drugs Aging* **1992**, *2*, 345–355.
- (28) Perry, S. W.; Hamilton, J. A.; Tjoelker, L. W.; Dbaibo, G.; Dzenko, K. A.; Epstein, L. G.; Hannun, Y.; Whittaker, J. S.; Dewhurst, S.; Gelbard, H. A. Platelet-activating factor receptor activation. An initiator step in HIV-1 neuropathogenesis. *J. Biol. Chem.* **1998**, *273*, 17660–17664.
- (29) Kato, K.; Clark, G. D.; Bazan, N. G.; Zorumski, C. F. Platelet-activating factor as a potential retrograde messenger in CA1 hippocampal long-term potentiation. *Nature* **1994**, *367*, 175–179.
- (30) Kordecki, E.; Wieraszko, A.; Chan, J. C.; Ehrlich, Y. H. Platelet activating factor (PAF) in memory formation: Role as a retrograde messenger in long-term potentiation. *J. Lipid Mediators Cell Signalling* **1996**, *14*, 115–126.
- (31) Chen, C.; Magee, J. C.; Marcheselli, V.; Hardy, M.; Bazan, N. G. Attenuated LTP in hippocampal dentate gyrus neurons of mice deficient in the PAF receptor. *J. Neurophysiol.* **2001**, *85*, 384–390.
- (32) Kobayashi, K.; Ishii, S.; Kume, K.; Takahashi, T.; Shimizu, T.; Manabe, T. Platelet-activating factor receptor is not required for long-term potentiation in the hippocampal CA1 region. *Eur. J. Neurosci.* **1999**, *11*, 1313–1316.
- (33) Smith, P. F.; MacLennan, K.; Darlington, C. L. The neuroprotective properties of the *Ginkgo biloba* leaf: a review of the possible relationship to platelet-activating factor (PAF). *J. Ethnopharmacol.* **1996**, *50*, 131–139.
- (34) Smith, P. F.; MacLennan, K. The therapeutic potential of PAF receptor antagonists in CNS disorders. *Curr. Opin. Anti-Inflammatory Immunomodulatory Invest. Drugs* **1999**, *1*, 205–218.
- (35) Corey, E. J.; Ghosh, A. K. Total synthesis of ginkgolide A. *Tetrahedron Lett.* **1988**, *29*, 3205–3206.
- (36) Corey, E. J.; Kang, M. C.; Desai, M. C.; Ghosh, A. K.; Houpis, I. N. Total synthesis of (±)-ginkgolide B. *J. Am. Chem. Soc.* **1988**, *110*, 649–651.
- (37) Corey, E. J.; Su, W. G. Total synthesis of a C_{15} ginkgolide, (±)-bilobalide. *J. Am. Chem. Soc.* **1987**, *109*, 7534–7536.
- (38) Corey, E. J.; Gavai, A. V. Simple analogues of ginkgolide B which are highly active antagonists of platelet activating factor. *Tetrahedron Lett.* **1989**, *30*, 6959–6962.
- (39) Corey, E. J.; Rao, K. S. Enantioselective total synthesis of ginkgolide derivatives lacking the *tert*-butyl group, an essential structural subunit for antagonism of platelet activating factor. *Tetrahedron Lett.* **1991**, *32*, 4623–4626.
- (40) Park, P.-U.; Pyo, S.; Lee, S.-K.; Sung, J. H.; Kwak, W. J.; Park, H.-K.; Cho, Y.-B.; Ryu, G. H.; Kim, T. S. Ginkgolide derivatives. U.S. Patent 5,541,183, 1996.
- (41) Hu, L.; Chen, Z.; Cheng, X.; Xie, Y. Chemistry of ginkgolides: structure–activity relationship as PAF antagonists. *Pure Appl. Chem.* **1999**, *71*, 1153–1156.
- (42) Hu, L.; Chen, Z.; Xie, Y.; Jiang, H.; Zhen, H. Alkyl and alkoxy-carbonyl derivatives of ginkgolide B: synthesis and biological evaluation of PAF inhibitory activity. *Bioorg. Med. Chem.* **2000**, *8*, 1515–1521.
- (43) Hu, L.; Chen, Z.; Xie, Y.; Jiang, Y.; Zhen, H. New products from alkali fusion of ginkgolides A and B. *J. Asian Nat. Prod. Res.* **2000**, *2*, 103–110.
- (44) Hu, L.; Chen, Z.; Xie, Y. Synthesis and biological activity of amide derivatives of ginkgolide A. *J. Asian Nat. Prod. Res.* **2001**, *3*, 219–227.
- (45) Dorman, G.; Prestwich, G. D. Using photolabile ligands in drug discovery and development. *Trends Biotechnol.* **2000**, *18*, 64–77.
- (46) Flemming, S. A. Chemical reagents in photoaffinity labeling. *Tetrahedron* **1995**, *51*, 12479–12520.
- (47) Kotzyba-Hilbert, F.; Kapfer, I.; Goeldner, M. Recent trends in photoaffinity labeling. *Angew. Chem., Int. Ed. Engl.* **1995**, *34*, 1296–1312.
- (48) Nassal, M. 4-(1-Azi-2,2,2-trifluoroethyl)benzoic acid, a highly photolabile carbene generating label readily fixable to biochemical agents. *Liebigs Ann. Chem.* **1983**, 1510–1523.
- (49) Nassal, M. 4-(1-Azi-2,2,2-trifluoroethyl)phenylalanine, a photolabile carbene-generating analogue of phenylalanine. *J. Am. Chem. Soc.* **1984**, *106*, 7540–7545.
- (50) Keana, J. F. W.; Cai, S. X. New reagents for photoaffinity labeling: synthesis and photolysis of functionalized perfluorophenyl azides. *J. Org. Chem.* **1990**, *55*, 3640–3647.
- (51) Lei, H.; Marks, V.; Pasquale, T.; Atkinson, J. K. Synthesis of photoaffinity label analogues of α -tocopherol. *Bioorg. Med. Chem. Lett.* **1998**, *8*, 3453–3458.
- (52) Lei, H.; Atkinson, J. Synthesis of phytyl- and chroman-derivatized photoaffinity labels based on α -tocopherol. *J. Org. Chem.* **2000**, *65*, 2560–2567.
- (53) Shindou, H.; Ishii, S.; Uozumi, N.; Shimizu, T. Roles of cytosolic phospholipase A2 and platelet-activating factor receptor in the Ca-induced biosynthesis of PAF. *Biochem. Biophys. Res. Commun.* **2000**, *271*, 812–817.
- (54) Li, H.; Liu, Y.; Fang, K.; Nakanishi, K. A simple photoaffinity labeling protocol. *Chem. Commun.* **1999**, 365–366.
- (55) MacLennan, K. M.; Smith, P. F.; Darlington, C. L. The effects of ginkgolide B (BN52021) on guinea pig vestibular nucleus neurons in vitro: importance of controlling for effects of dimethyl sulfoxide (DMSO) vehicles. *Neurosci. Res.* **1996**, *26*, 395–399.
- (56) Fukunaga, K.; Ishii, S.; Asano, K.; Yokomizo, T.; Shiomi, T.; Shimizu, T.; Yamaguchi, K. Single nucleotide polymorphism of human platelet-activating factor receptor impairs G-protein activation. *J. Biol. Chem.* **2001**, *276*, 43025–43030.
- (57) Aoki, Y.; Nakamura, M.; Kodama, H.; Matsumoto, T.; Shimizu, T.; Noma, M. A radioreceptor binding assay for platelet-activating factor (PAF) using membranes from CHO cells expressing human PAF receptor. *J. Immunol. Methods* **1995**, *186*, 225–231.
- (58) Corey, E. J.; Rao, K. S.; Ghosh, A. K. Intramolecular and intermolecular hydroxyl reactivity differences in ginkgolides A, B and C and their chemical applications. *Tetrahedron Lett.* **1992**, *33*, 6955–6958.
- (59) Weinges, K.; Schick, H. Chemie der Ginkgolide IV. Herstellung von Ginkgolide B aus Ginkgolide C. *Liebigs Ann. Chem.* **1991**, 81–83.
- (60) Chen, J.; Hu, L.; Jiang, H.; Gu, J.; Zhu, W.; Chen, Z.; Chen, K.; Ji, R. A 3D-QSAR study on ginkgolides and their analogues with comparative molecular field analysis. *Bioorg. Med. Chem. Lett.* **1998**, *8*, 1291–1296.
- (61) van Beek, T. A.; Lelyved, G. P. Preparative isolation and separation procedure for ginkgolides A, B, C, and J and bilobalide. *J. Nat. Prod.* **1997**, *60*, 735–738.
- (62) Ishii, S.; Nagase, T.; Tashiro, F.; Ikuta, K.; Sato, S.; Waga, I.; Kume, K.; Miyazaki, J.; Shimizu, T. Bronchial hyperreactivity, increased endotoxin lethality and melanocytic tumorigenesis in transgenic mice overexpressing platelet-activating factor receptor. *EMBO J.* **1997**, *16*, 133–142.
- (63) Bradford, M. M. A rapid and sensitive method for the quantitation of microgram quantities of protein utilizing the principle of protein-dye binding. *Anal. Biochem.* **1976**, *72*, 248–254.
- (64) Cheng, Y.; Prusoff, W. H. Relationship between the inhibition constant (K_i) and the concentration of inhibitor which causes 50% inhibition (I_{50}) of an enzymatic reaction. *Biochem. Pharmacol.* **1973**, *22*, 3099–3103.

JM020147W

Block of the background K⁺ channel TASK-1 contributes to arrhythmogenic effects of platelet-activating factor

ANDREA BARBUTI,¹ SATOSHI ISHII,² TAKAO SHIMIZU,²
RICHARD B. ROBINSON,¹ AND STEVEN J. FEINMARK¹

¹Center for Molecular Therapeutics, Department of Pharmacology,
Columbia University, New York, New York 10032; and ²Department
of Biochemistry and Molecular Biology, University of Tokyo, Tokyo, 113-003 Japan

Received 2 November 2001; accepted in final form 30 January 2002

Barbuti, Andrea, Satoshi Ishii, Takao Shimizu, Richard B. Robinson, and Steven J. Feinmark. Block of the background K⁺ channel TASK-1 contributes to arrhythmogenic effects of platelet-activating factor. *Am J Physiol Heart Circ Physiol* 282: H2024–H2030, 2002. First published January 31, 2002; 10.1152/ajpheart.00956.2001.—Platelet-activating factor (PAF), an inflammatory phospholipid, induces ventricular arrhythmia via an unknown ionic mechanism. We can now link PAF-mediated cardiac electrophysiological effects to inhibition of a two-pore domain K⁺ channel [TWIK-related acid-sensitive K⁺ background channel (TASK-1)]. Superfusion of carbamyl-PAF (C-PAF), a stable analog of PAF, over murine ventricular myocytes causes abnormal automaticity, plateau phase arrest of the action potential, and early afterdepolarizations in paced and quiescent cells from wild-type but not PAF receptor knockout mice. C-PAF-dependent currents are insensitive to Cs⁺ and are outwardly rectifying with biophysical properties consistent with a K⁺-selective channel. The current is blocked by TASK-1 inhibitors, including protons, Ba²⁺, Zn²⁺, and methanandamide, a stable analog of the endogenous lipid ligand of cannabinoid receptors. In addition, when TASK-1 is expressed in CHO cells that express an endogenous PAF receptor, superfusion of C-PAF decreases the expressed current. Like C-PAF, methanandamide evoked spontaneous activity in quiescent myocytes. C-PAF- and methanandamide-sensitive currents are blocked by a specific protein kinase C (PKC) inhibitor, implying overlapping signaling pathways. In conclusion, C-PAF blocks TASK-1 or a closely related channel, the effect is PKC dependent, and the inhibition alters the electrical activity of myocytes in ways that would be arrhythmogenic in the intact heart.

two-pore domain potassium channels; Kenk3 ventricular myocytes; inflammatory lipids; mouse

LETHAL ARRHYTHMIAS commonly occur after myocardial ischemia, especially when the ischemic myocardium is reperfused. These arrhythmias are usually initiated by ectopic activity triggered by early (EADs) and delayed afterdepolarizations (DADs) of the membrane potential. One consequence of ischemia and reperfusion is a

rapid migration of polymorphonuclear leukocytes (PMNL) into the infarcted zone. Activated PMNL bind to activated myocytes and release several substances, including oxygen radicals, proteolytic enzymes, and inflammatory lipids that increase the extent of myocardial injury (15). Depletion of circulating neutrophils or treatment with anti-inflammatory drugs effectively limits the size of the infarct zone and the extent of the damage in hearts from several species (15, 20, 22)

Hoffman et al. (4, 5) demonstrated that activation of PMNL bound to isolated canine myocytes dramatically changed the myocyte transmembrane action potential. These changes included prolongation of the action potential duration (APD), EADs, and in some cases arrest during the plateau phase of the action potential. It was also shown that direct superfusion of myocytes with the inflammatory phospholipid platelet-activating factor (PAF) mimicked the action of activated PMNL and that, under similar conditions, PMNL produce significant levels of PAF. Furthermore, incubation of myocytes with the PAF receptor (PAFR) antagonist CV-6209 prevented both PAF- and PMNL-induced changes in myocyte membrane potential. PAF also induces arrhythmias in mice that overexpress the PAFR when the lipid is administered at intravenous doses that have little effect on wild-type (WT) animals (7). These observations suggested that PMNL-derived PAF could induce triggered activity and thus ventricular arrhythmias.

There is considerable confusion regarding the molecular mechanisms by which PAF could alter the electrical activity of the heart. Although PAF binds to a cell surface, G protein-linked receptor and ultimately increases cytosolic Ca²⁺ levels (17, 19), little is known about the effects of PAF on membrane channels. Wahler et al. (26) showed that subnanomolar concentrations of PAF markedly decreased the inwardly rectifying K⁺ channel (*I_{K1}*) in guinea pig ventricular myocytes, whereas Hoffman et al. (5) suggested that depolarizing Na⁺ current may play a role in the arrhythmogenic action of PAF.

Address for reprint requests and other correspondence: S. J. Feinmark, Center for Molecular Therapeutics, Dept. of Pharmacology, Columbia Univ., 630 W168th St., New York, NY 10032 (E-mail: sjf1@columbia.edu).

The costs of publication of this article were defrayed in part by the payment of page charges. The article must therefore be hereby marked "advertisement" in accordance with 18 U.S.C. Section 1734 solely to indicate this fact.

Taking advantage of genetically modified mice in which PAFR have been knocked out [knockout (KO) mice] (6), we tested the ability of carbamyl-PAF (C-PAF), a nonmetabolizable PAF analog, to alter the membrane potential of isolated murine ventricular myocytes with the intent of clarifying the mechanisms determining the arrhythmogenic effects of this lipid.

METHODS

Cell preparation. Adult mice, 2–3 mo old, were anesthetized with ketamine-xylazine, and their hearts were removed according to protocols approved by the Columbia University Institutional Animal Care and Use Committee. Experiments were performed on single, rod-shaped, quiescent ventricular myocytes dissociated using a standard retrograde collagenase perfusion (11) from hearts of mice that were either WT or PAFR KO. Both WT and KO mice were bred on a C57/B16 background. The derivation of the KO mice has been described previously (5).

Heterologous expression. The TWIK-related acid-sensitive K^+ background channel (TASK-1) clone (provided by Professor Y. Kurachi, Osaka University; Osaka, Japan) was cotransfected in CHO cells with CD8 plasmid using Lipofectamine Plus (Invitrogen) according to the manufacturer's instructions. Forty-eight hours later, cells were transferred to the electrophysiology chamber, and anti-CD8-coated beads (DynaL Biotech) were added to identify CD8-expressing cells. The CD8-expressing cells were voltage clamped using a ramp clamp (see *Electrophysiological recordings*). CHO cells were used in these experiments in part because they express endogenous PAFR.

Buffers and drugs. Before electrophysiological measurements, cells were placed into the perfusion chamber and superfused at room temperature with Tyrode buffer [containing (in mM) 140 NaCl, 5.4 KCl, 1 CaCl₂, 1 MgCl₂, 5 HEPES, and 10 glucose; pH 7.4]. The whole cell patch-clamp technique was used with pipettes having resistances of 1.5–3 M Ω [the intracellular solution contained (in mM) 130 aspartic acid, 146 KOH, 10 NaCl, 2 CaCl₂, 5 EGTA, 10 HEPES, and 2 MgATP; pH 7.2]. Solutions of C-PAF, the PAFR antagonist CV-6209 (BIOMOL), and the protein kinase C (PKC) inhibi-

tor bisindolylmaleimide I (BIM I; Calbiochem) were prepared in water and diluted in Tyrode buffer before use. An inactive analog of BIM I (BIM V; Calbiochem), anandamide, its non-hydrolyzable analog, methanandamide, and an inhibitor of anandamide hydrolysis, arachidonyltrifluoromethyl ketone (ATFK) (BIOMOL), were dissolved in DMSO and then diluted in Tyrode buffer. The final DMSO concentration did not exceed 0.1%. A custom-made fast perfusion device was used to exchange the solution around the cell within 1 s (2).

Electrophysiological recordings. Current and voltage protocols were generated using Clampex 7.0 software applied by means of an Axopatch 200B amplifier and a Digidata 1200 interface (Axon Instruments). During voltage clamp, steady-state current traces were acquired at 500 Hz and final filtered at 10 Hz. During current clamp, membrane voltage was acquired at 5 kHz and filtered at 1 kHz. Ramp clamps were conducted by imposing a voltage ramp (14 mV/s) at an acquisition rate of 500 Hz with 1-kHz filtering. Data were analyzed using pCLAMP 8.0 (Axon) and Origin 6.0 (Microcal) and are presented as means \pm SE. Steady-state current was determined by computer calculation of average current over a time period of at least 5 s. In all experiments, the n value indicates the number of myocytes studied and represents pooled data from at least two (voltage clamp) or three (current clamp) animals. Student's t -test, one-way ANOVA, and χ^2 -tests were used; a value of $P < 0.05$ was considered statistically significant. Records have been corrected for the junction potential, which was measured to be 9.8 mV.

RESULTS

C-PAF alters the rhythm of paced, WT ventricular myocytes. Myocytes from WT mice were paced (cycle length, 1,000 ms) and monitored in current-clamp mode to record action potentials. When the APD was stable for 2 min, cells were superfused with 185 nM C-PAF (Fig. 1), a concentration that elicited electrophysiological effects in 9 of 11 cells. C-PAF-evoked responses occurred after a delay (94 ± 21 s; range, 23–184 s) and typically included abnormal automaticity (Fig. 1; 110 s) leading to a maintained depolariza-

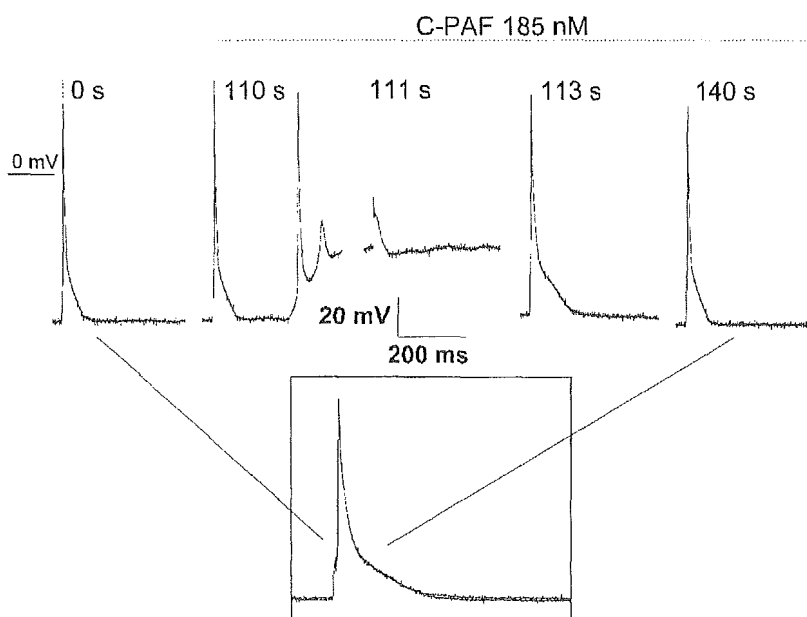


Fig. 1. Carbamyl-platelet-activating factor (C-PAF) alters normal action potentials in mouse ventricular myocytes. Paced action potentials (cycle length, 1,000 ms) were recorded in current-clamp mode under control conditions (0 s) and after perfusion of C-PAF (185 nM). After a delay, C-PAF caused abnormal automaticity (110 s) and sustained depolarization (111 s). The action potential progressively shortened and normal rhythm was reestablished, indicating desensitization of the receptor in continuous presence of drug (113 and 140 s). *Inset:* traces during control perfusion and after recovery completely overlap. The data are derived from a single cell and are typical of 8 cells. The traces were recorded immediately before the application of C-PAF (0 s) and 110, 111, 113, and 140 s after C-PAF application.

tion (Fig. 1; 111 s). In eight of nine cells, alteration of the membrane potential slowly returned to normal, presumably due to receptor desensitization, and after 3 min of agonist perfusion was indistinguishable from that of controls (Fig. 1, inset).

C-PAF decreases an outward current that is K^+ selective and carried by TASK-1. Cells were held at -10 mV, and total steady-state membrane currents were measured. The mean holding current was 133 ± 12 pA ($n = 24$). WT myocytes responded to C-PAF with decreased net outward current that often began to reverse during the perfusion and recovered completely after washout (Fig. 2A). Because a depolarizing shift in steady-state current can be caused by increased inward currents or decreased outward currents, we determined how C-PAF affected conductance. When a $+10$ -mV step was applied during control and agonist superfusion, we found that C-PAF decreased conductance $17.5 \pm 3.9\%$ ($n = 5$, $P < 0.05$), indicating that the lipid inhibits outward currents. The main conductance maintaining resting potential in the ventricle is I_{K1} ; therefore, we tested whether this inwardly rectifying K^+ current was involved in the action of C-PAF. Cs^+ (5 mM), which largely blocks I_{K1} under these conditions (data not shown), did not reduce the C-PAF-sensitive current in cells held at -70 mV. The average C-PAF-sensitive current density was 0.047 ± 0.01 pA/pF in control cells compared with 0.047 ± 0.03 pA/pF in cells in the presence of Cs^+ ($n = 6$). By extending the voltage-clamp study to other potentials, we obtained a nearly linear current-voltage relation for the C-PAF difference current (Fig. 2B, ■). In KO myocytes, the C-PAF-sensitive current was absent at all potentials tested (Fig. 2B, ●).

We did not observe a clear reversal potential in physiological K^+ over the voltage range tested. Therefore, we conducted additional experiments in elevated extracellular K^+ [50 mM K^+ , with Na^+ reduced to 100 mM, plus 5 mM Cs^+ and 1 mM tetraethylammonium ion (TEA^+)] designed to measure the reversal potential of the C-PAF-sensitive current. In elevated extracellular K^+ , our results show a weakly outward rectifying current with a current-voltage relation that is consistent with that of a predominantly K^+ -selective channel (Fig. 2C). The calculated K^+ equilibrium potential for these recording conditions is -27.6 mV, and the observed reversal for the C-PAF-sensitive current occurred at -20.4 ± 3 mV ($n = 5$).

The C-PAF-sensitive current was blocked by the PAFR antagonist CV-6209 (100 nM; Fig. 3). The lack of a C-PAF-dependent response in the presence of CV-6209 was identical to the results obtained in myocytes derived from KO mice (Fig. 3). Taken together, these results confirm that the C-PAF effect is mediated by the PAFR and involves inhibition of an outward K^+ current distinct from I_{K1} .

These characteristics of the C-PAF-sensitive current suggested that it may be mediated by a member of the "two-pore domain" K^+ channel family (13). TASK-1 is a member of this family that is expressed in the mammalian heart (9, 10, 13, 14). In heterologous expression

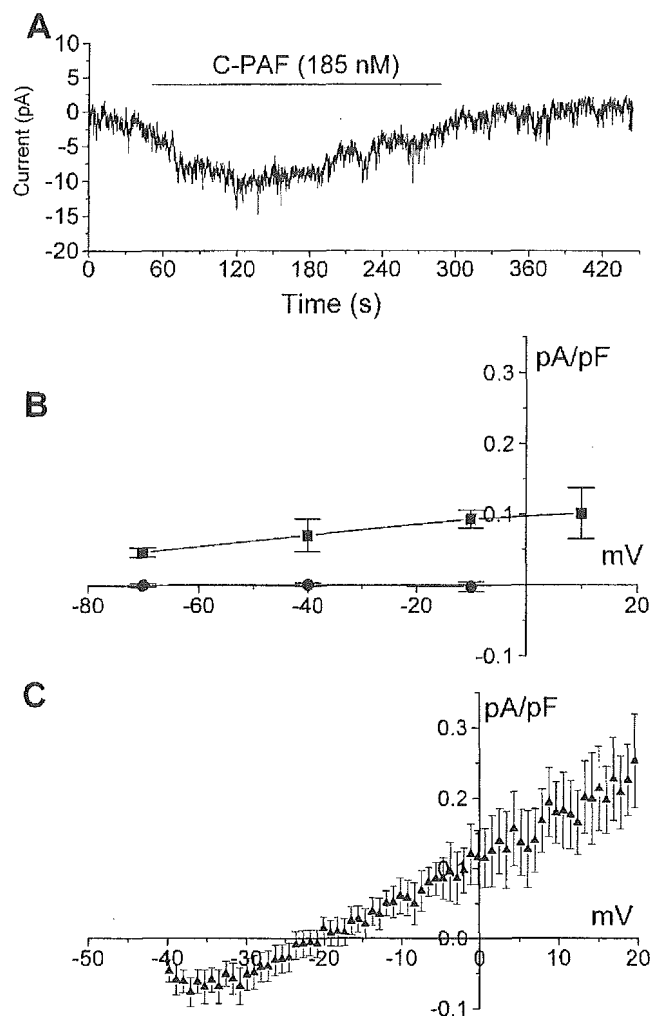


Fig. 2. Application of C-PAF causes a depolarizing shift in net membrane current in wild-type (WT) but not in knockout (KO) myocytes. Superfusion of C-PAF (185 nM) caused a transient decrease in the net outward current in a WT myocyte held at -10 mV (A). In this trace, the baseline outward holding current was adjusted to zero to illustrate the C-PAF-sensitive current. The spontaneous reversal of the C-PAF effect probably indicates desensitization of the PAF receptor (PAFR). The current (I)-voltage (V) relation of the C-PAF difference current (control minus C-PAF) is plotted as a net outward current over a range of potentials in WT myocytes (B, ■). In KO myocytes (●), no C-PAF-sensitive current was detected at all potentials tested. Each data point is the mean \pm SE of data from at least 4 cells at each potential. The I - V relation was also measured using a ramp protocol in high extracellular K^+ (50 mM) plus Cs^+ (5 mM) and tetraethylammonium ion (1 mM) to permit determination of the reversal potential (C). Each data point is the mean \pm SE of data from at least 5 cells from 2 animals.

systems, this channel is outwardly rectifying and is blocked by H^+ , Ba^{2+} , Zn^{2+} , and anandamide, an endogenous cannabinoid receptor ligand (9, 10, 13, 14, 16, 18, 24). Consistent with this, in isolated myocytes, when the external pH was lowered to 6.4 or when Ba^{2+} (3 mM) or Zn^{2+} (3 mM) was present, the C-PAF-sensitive current was significantly reduced (Fig. 4). Methanandamide (10 μ M), a stable analog of anandamide, also inhibited the C-PAF-sensitive current (Fig. 4). In contrast, anandamide inhibition was only significant in the presence of ATRF (10 μ M), an inhibitor of

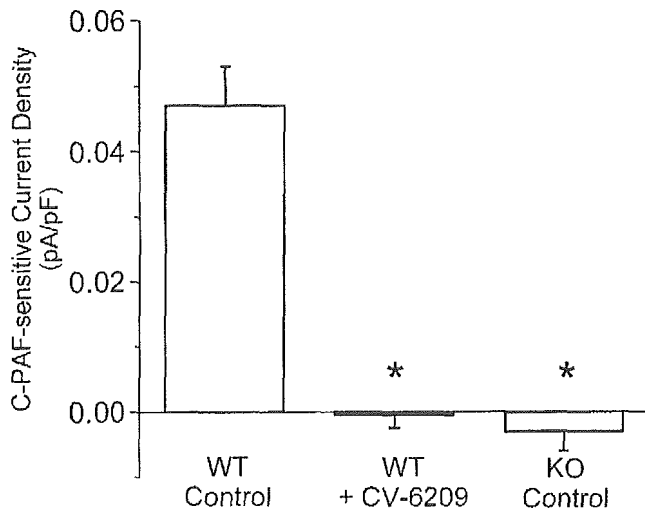


Fig. 3. The C-PAF-sensitive current is receptor mediated. The C-PAF-sensitive current was measured in WT myocytes held at -70 mV under various conditions. The current under control conditions in WT myocytes disappeared in the presence of the PAFR antagonist CV-6209 (100 nM, $n = 5$). There was no C-PAF-sensitive current detected in myocytes from KO mice ($n = 3$). * $P < 0.01$.

anandamide hydrolysis (Fig. 4), suggesting rapid metabolism of anandamide by ventricular myocytes. ATRK alone had no effect (data not shown).

CHO cells expressing TASK-1 exhibited a large outwardly rectifying current that was pH sensitive. The mean current-voltage relation at alkaline and acidic

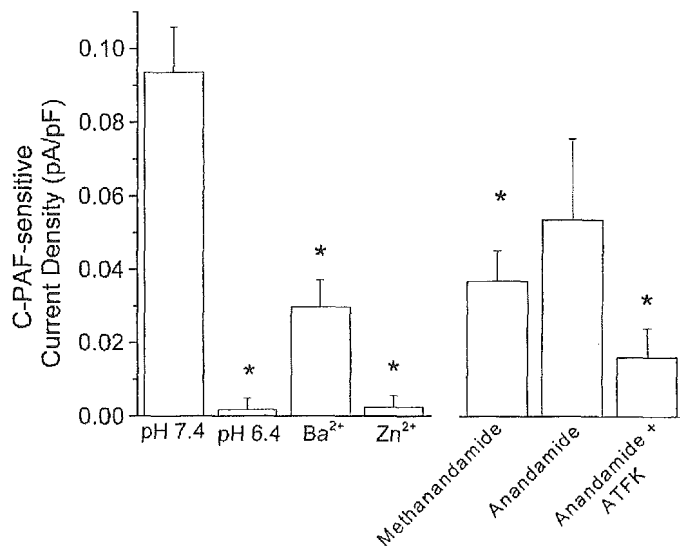


Fig. 4. Block of the TWIK-related acid-sensitive K⁺ background channel (TASK-1) decreases the C-PAF-sensitive steady-state current. WT myocytes were held at -10 mV, and the C-PAF-sensitive current was measured at pH 7.4 ($n = 25$). The change in net current elicited by C-PAF (185 nM) was significantly decreased in the presence of Tyrode buffer at pH 6.4 ($n = 6$), Ba²⁺ (3 mM, $n = 6$), or Zn²⁺ (3 mM, $n = 8$). The stable anandamide analog methanandamide (10 μ M, $n = 12$) also significantly reduced the C-PAF-sensitive current, as did anandamide in the presence of arachidonyltrifluoromethyl ketone (ATRK), a drug that inhibits anandamide metabolism (10 μ M, $n = 8$). Anandamide alone did not significantly inhibit the current (10 μ M, $n = 5$) due to its rapid metabolic inactivation. * $P < 0.05$ compared with control at pH 7.4.

pH is shown in Fig. 5, left, and demonstrates that the reduction of the external pH to 6 completely eliminated the outwardly rectifying current. Mean current density at $+30$ mV in cells expressing TASK-1 was 26 pA/pF compared with 0.6 pA/pF for nontransfected cells. When TASK-1-transfected CHO cells were superfused with C-PAF (185 nM), the expressed current was reduced (Fig. 5, right), demonstrating the inhibitory effect of C-PAF on TASK-1-dependent current.

If both C-PAF and methanandamide block TASK-1, then methanandamide itself should cause a decreased net outward current. Thus the methanandamide-sensitive current was measured (Fig. 6). Because this current is comparable to the C-PAF-sensitive current, we also asked whether the methanandamide-sensitive current was mediated by the PAFR and found that the lipid was fully effective in the presence of the PAFR antagonist CV-6209 or when applied to myocytes from KO mice (Fig. 6). Thus the effect of methanandamide is not mediated by the PAFR.

C-PAF action involves PKC-dependent block of TASK-1. In many cell types, PAF initiates an intracellular pathway that results in activation of PKC (1, 17, 19, 23). To determine whether C-PAF initiates this cascade in ventricular myocytes, we incubated cells with BIM I, a selective PKC inhibitor (25) [inhibitory constant, 14 nM], before applying C-PAF. The C-PAF-sensitive current was blocked in a dose-dependent manner (Fig. 7, A and B) by BIM I but was not altered by the addition of an inactive analog, BIM V. The inhibition occurred in a voltage-independent manner (Fig. 7C).

We then asked whether the methanandamide-sensitive current also required PKC activity. BIM I (100 nM) significantly reduced the methanandamide-sensi-

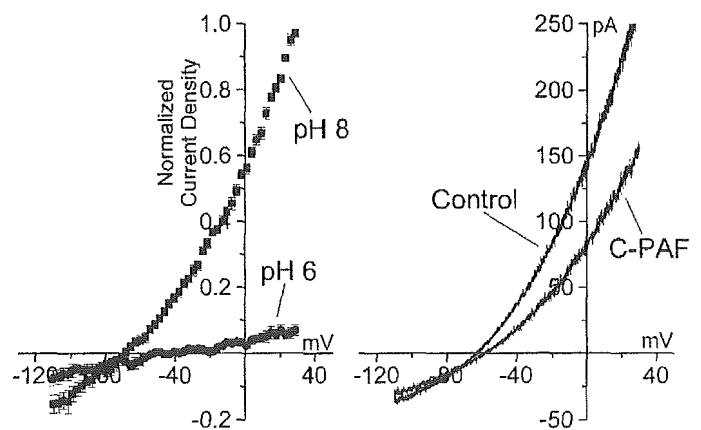


Fig. 5. TASK-1 heterologously expressed in CHO cells is sensitive to pH and to C-PAF. Net steady-state current was measured by a ramp clamp under alkaline (pH 8) and acidic (pH 6) conditions, demonstrating the pH sensitivity of the expressed TASK-1 current. The I - V relation of each cell was normalized to the current at 30 mV to correct for cell-to-cell variability in expression levels, and the mean normalized current density was plotted (left, $n = 13$). In CHO cells exposed to C-PAF (185 nM), the expressed TASK-1 current was decreased (right). Representative I - V relations before (control) and during drug treatment (C-PAF) were compared. This result is representative of 8 cells. On average, the I - V relation returned to within 5% of control value after washout of C-PAF.

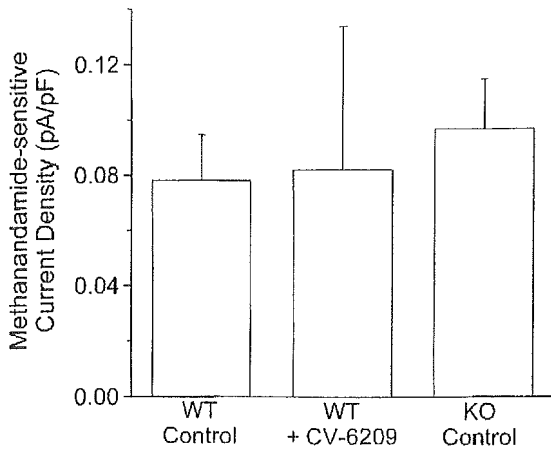


Fig. 6. The methanandamide-sensitive current is independent of the PAFR. WT cells held at -10 mV were superfused with methanandamide ($10 \mu\text{M}$), and the methanandamide-sensitive current was measured (WT control, $n = 6$). The methanandamide-sensitive current did not differ from control when WT cells were incubated with the PAFR antagonist CV-6209 (100 nM, $n = 3$) or in myocytes derived from PAFR knockout mice (KO control, $n = 6$).

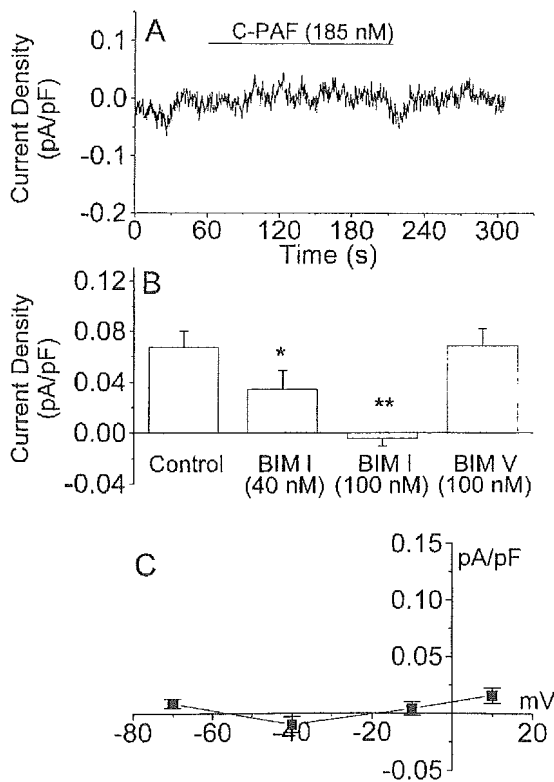


Fig. 7. The C-PAF-sensitive current is blocked by inhibition of protein kinase C (PKC). The C-PAF-sensitive current was completely blocked in myocytes (held at -10 mV) exposed to bisindolylmaleimide I (BIM I), a specific PKC inhibitor (100 nM; A). In this trace, the baseline holding current was adjusted to zero to illustrate the absence of a C-PAF-sensitive current. BIM I-mediated inhibition of the C-PAF-sensitive current is dose dependent (B; 40 nM, $n = 7$, and 100 nM, $n = 11$). An inactive BIM I analog, BIM V, does not block the C-PAF-sensitive current (B; $n = 10$). The inhibition of the C-PAF-sensitive current by BIM I is independent of voltage (C; 100 nM BIM I, $n =$ at least 4 for each data point). * $P < 0.05$ and ** $P < 0.001$ vs. control.

tive current in WT myocytes ($P < 0.05$, $n = 5$; data not shown).

C-PAF and methanandamide induce spontaneous activity in quiescent myocytes. Because C-PAF and methanandamide affect net steady-state current at voltages near the resting potential, we asked whether electrophysiological effects occurred independent of pacing. Membrane potential was recorded from myocytes that remained quiescent for at least 2 min. Every WT quiescent myocyte tested was sensitive to C-PAF superfusion (11 of 11 cells; Fig. 8A), typically responding with an action potential that arrested in the plateau phase (Fig. 8A, inset), and exhibited many small fluctuations of the membrane potential and EAD. Eventually, the membrane repolarized. The duration of the effect was variable, but its appearance always followed an initial delay (96 ± 11 s). In contrast, when C-PAF was applied to ventricular myocytes isolated from PAFR KO mice, there was no response in most of the cells (7 of 9 cells;

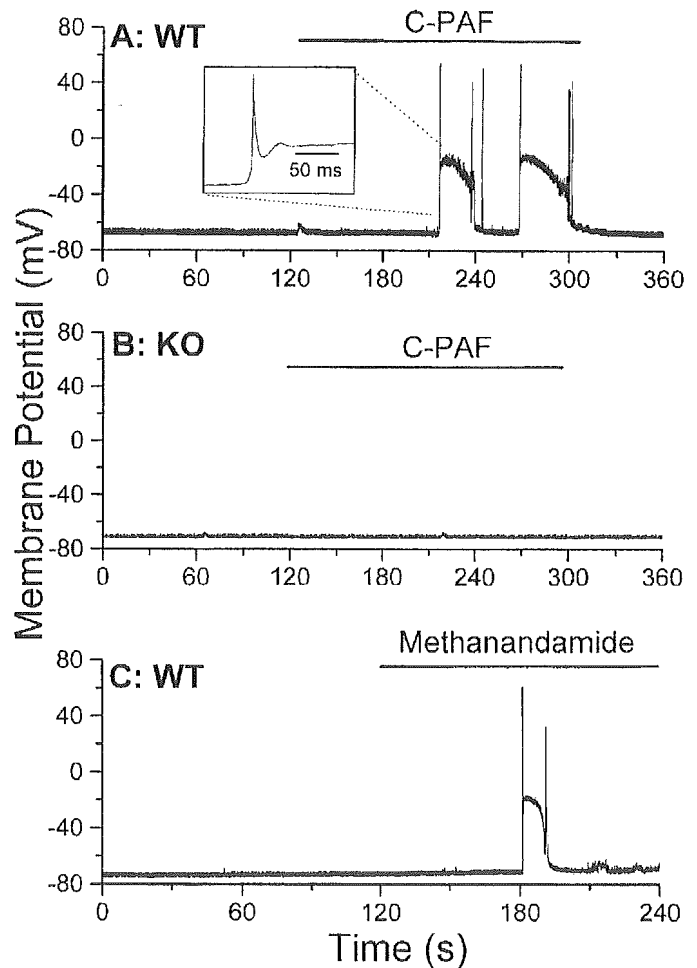


Fig. 8. C-PAF and methanandamide elicit spontaneous activity in quiescent WT myocytes. Quiescent myocytes from WT and KO mice were studied in current-clamp mode. C-PAF (185 nM) application elicited spontaneous activity in WT (A) but not KO myocytes (B). Superfusion of methanandamide ($10 \mu\text{M}$) over WT myocytes caused the same effect as C-PAF (C). There was no measurable change in the resting potential before impulse initiation. These recordings are typical of 11 cells for A, 7 cells for B, and 7 cells for C.

Fig. 8B). The responsiveness of WT and KO myocytes to C-PAF differed significantly ($P < 0.01$, $\chi^2 = 9.96$), although their resting potentials did not (-70.6 ± 1.1 vs. -71.3 ± 1.5 mV). Finally, six of eight quiescent WT cells failed to respond to C-PAF (185 nM) after BIM I treatment (100 nM). A comparison of BIM-treated to control myocytes indicated a significant reduction in susceptibility to spontaneous activity ($P < 0.01$, $\chi^2 = 8.84$).

If the decrease in outward current caused by blocking the TASK-1 channel is related to the arrhythmogenic effects of C-PAF, application of a TASK-1 inhibitor in current-clamp mode should mimic the effects of C-PAF and evoke spontaneous activity. Accordingly, when methanandamide was applied to quiescent WT myocytes, spontaneous action potentials were observed (7 of 12 cells; Fig. 8C). Statistical analysis showed no difference in the occurrence of spontaneous activity during methanandamide compared with C-PAF superfusion.

DISCUSSION

Inflammatory products released by PMNL can have negative effects on cardiac function and the survival of areas at risk after periods of ischemia and reperfusion (15). Our earlier studies in isolated canine ventricular myocytes (4) demonstrated that PAF, a PMNL-derived inflammatory lipid, could alter action potentials by prolongation of the APD, EADs, and arrest at the plateau. The present study demonstrates that in murine ventricular myocytes, C-PAF also triggers a series of alterations in action potentials, including spontaneous beats, EADs, and prolonged depolarization similar to those observed in canine myocytes (4, 5). This supports the validity of the mouse as a model in which to study the molecular basis of the arrhythmogenic effect of PAF.

We measured changes in the membrane potential, spontaneous activity, and in specific ion currents in myocytes as they were exposed to C-PAF. This lipid causes a small change in net current that develops over the first minute after application. Changes in the action potential (or appearance of spontaneous action potentials in quiescent cells) lag behind the peak current by ~ 20 s (at -70 mV, the C-PAF-sensitive current peaked by 74 ± 13 s). The generation of spontaneous activity in quiescent myocytes implies that changes in membrane potential are not strictly dependent on the stimulus or alterations in active currents but rather that it is likely that the agonist perturbs the balance among those currents active at the resting membrane potential. Voltage-clamp experiments measuring changes in conductance indicate that C-PAF effects are dependent on a decrease in outward currents. In addition, the C-PAF-sensitive current, measured in elevated K^+ , showed weak outward rectification and had a reversal potential close to the calculated K^+ equilibrium potential. These data indicate that the C-PAF-sensitive current is largely carried by K^+ .

Because experiments utilizing Cs^+ argue against the involvement of I_{K1} in the ionic mechanism underlying the PAF-sensitive current, our attention shifted to other K^+ channels that are active at rest. The two-pore domain K^+ channels (13) are voltage- and time-independent background channels having characteristics similar to the channel responsible for the C-PAF-sensitive current. Within this family, TASK-1 [also referred to as cTBAK-1 (9) and Kcnk3 (14)] is expressed in the heart (10). TASK-1 is sensitive to small variations in external pH and is almost completely inhibited at pH 6.4. It is also blocked by Ba^{2+} or Zn^{2+} and by the putative endogenous lipid ligand of the cannabinoid receptors anandamide (16). The C-PAF-sensitive current in murine ventricular myocytes was sensitive to all these interventions, suggesting that C-PAF-mediated effects are associated with inhibition of TASK-1 or a closely related channel. Confirmation that the TASK-1 channel is sensitive to C-PAF was obtained by expressing TASK-1 in CHO cells. When TASK-1-expressing CHO cells were superfused with C-PAF, the expressed current was reduced.

Because our data suggested that the C-PAF-sensitive current is due to TASK-1 blockade, we reasoned that anandamide treatment might prevent myocytes from responding to C-PAF. In fact, both anandamide in the presence of ATRF, an inhibitor of anandamide hydrolysis, and its nonhydrolyzable analog, methanandamide, significantly reduced the C-PAF effect, confirming our hypothesis. It follows that if C-PAF and methanandamide both inhibit TASK-1 and if this is the ionic basis for the C-PAF-sensitive effects, methanandamide should induce similar changes in myocyte physiology. As predicted, methanandamide caused both a decrease in net outward current and an increase in spontaneous activity in quiescent myocytes. Therefore, we conclude that both C-PAF and methanandamide exert their biological effects at least in part by inhibiting TASK-1 or a closely related channel.

In a heterologous expression system, Maingret et al. (16) found that anandamide inhibition of TASK-1 was not mediated by the known cannabinoid receptors, and, because the drug was effective on excised macropatches, they concluded that the lipid interacted directly with the channel. PAF, in contrast, is known to activate cells through a G protein-linked receptor that initiates a signaling cascade involving activation of phospholipase C, generating inositol phosphates and elevating intracellular calcium and diacylglycerol, ultimately activating PKC (1, 8, 17, 19). In our studies, the effect of C-PAF is clearly mediated by the PAFR because its activity can be blocked by the antagonist CV-6209 and is absent in myocytes derived from mice in which the PAFR has been genetically deleted. In addition, we found that inhibition of PKC blocked the C-PAF-sensitive current. Although several reports suggest that TASK-1 is insensitive to PKC activators (3, 12), Lopes et al. (14) found that phorbol 12-myristate 13-acetate causes a slowly developing block of TASK-1 current in an oocyte expression system. This further supports our hypothesis that C-PAF activity is

mediated by activation of PKC-dependent phosphorylation, and, although it does not resolve the mechanism behind the somewhat unexpected time course of the effect, it is entirely consistent with our findings.

Interestingly, PKC inhibition also reduced the methanandamide-sensitive current, suggesting that the two lipids share overlapping intracellular signaling pathways. Therefore, we tested whether methanandamide required the PAFR for its activity and found that it was fully functional in the presence of CV-6209 and in myocytes derived from KO mice. These data suggest that the methanandamide effect is dependent, at least in part, on PKC activation. Alternatively, the block of the TASK-1 channel by methanandamide may require a basal phosphorylation of the channel itself or an accessory protein and thus ultimately depends on, but is not mediated by, PKC. Such a scenario was recently described for a similar effect of anandamide on the VR₁ vanilloid receptor, a nonselective cation channel. In this case, activation of the receptor by anandamide was significantly enhanced when the channel had been phosphorylated by PKC, and anandamide itself stimulated PKC (21).

These results suggest, for the first time, a role for the TASK-1 channel in PAF-mediated arrhythmias. However, additional questions remain. While block of TASK-1 channels could contribute to a longer APD and subsequent EADs, this does not preclude additional effects on other currents active during the action potential plateau, including Ca²⁺, Na⁺, and the delayed rectifier currents. In addition, the mechanism by which TASK-1 blockade might lead to initiation of spontaneous activity in a quiescent myocyte is not clear, because no measurable change in membrane potential was observed immediately preceding initiation of activity induced by either C-PAF or methanandamide. Additional mechanisms, either secondary to the block of TASK-1 or independent of this action, may occur after exposure to PAF. The murine model, and its amenability to genetic manipulations, should prove useful in the ultimate resolution of these remaining questions.

The authors thank Irina Voloshyna and Patricia McLaughlin for excellent technical assistance and Dr. Michael R. Rosen for critical comments on the manuscript.

This work was supported by National Heart, Lung, and Blood Institute Grant HL-56140 and by a Servier Strategic Alliance.

REFERENCES

1. Chao W and Olson MS. Platelet-activating factor: receptors and signal transduction. *Biochem J* 292: 617–629, 1993.
2. DiFrancesco D, Ferroni A, Mazzanti M, and Tromba C. Properties of the hyperpolarizing-activated current (*i_p*) in cells isolated from the rabbit sino-atrial node. *J Physiol (Lond)* 377: 61–88, 1986.
3. Duprat F, Lesage F, Fink M, Reyes R, Heurteaux C, and Lazdunski M. TASK, a human background K⁺ channel to sense external pH variations near physiological pH. *EMBO J* 16: 5464–5471, 1997.
4. Hoffman BF, Feinmark SJ, and Guo SD. Electrophysiologic effects of interactions between activated canine neutrophils and cardiac myocytes. *J Cardiovasc Electrophysiol* 8: 679–687, 1997.
5. Hoffman BF, Guo SD, and Feinmark SJ. Arrhythmias caused by platelet activating factor. *J Cardiovasc Electrophysiol* 7: 120–133, 1996.
6. Ishii S, Kuwaki T, Nagase T, Maki K, Tashiro F, Sunaga S, Cao WH, Kume K, Fukuchi Y, Ikuta K, Miyazaki J, Kumada M, and Shimizu T. Impaired anaphylactic responses with intact sensitivity to endotoxin in mice lacking a platelet-activating factor receptor. *J Exp Med* 187: 1779–1788, 1998.
7. Ishii S, Nagase T, Tashiro F, Ikuta K, Sato S, Waga I, Kume K, Miyazaki J, and Shimizu T. Bronchial hyperreactivity, increased endotoxin lethality and melanocytic tumorigenesis in transgenic mice overexpressing platelet-activating factor receptor. *EMBO J* 16: 133–142, 1997.
8. Ishii S and Shimizu T. Platelet-activating factor (PAF) receptor and genetically engineered PAF receptor mutant mice. *Prog Lipid Res* 39: 41–82, 2000.
9. Kim D, Fujita A, Horio Y, and Kurachi Y. Cloning and functional expression of a novel cardiac two-pore background K⁺ channel (*κ*TBAK-1). *Circ Res* 82: 513–518, 1998.
10. Kim Y, Bang H, and Kim D. TBAK-1 and TASK-1, two-pore K⁺ channel subunits: kinetic properties and expression in rat heart. *Am J Physiol Heart Circ Physiol* 277: H1669–H1678, 1999.
11. Kuznetsov V, Pak E, Robinson RB, and Steinberg SF. β_2 -Adrenergic receptor actions in neonatal and adult rat ventricular myocytes. *Circ Res* 76: 40–52, 1995.
12. Leonoudakis D, Gray AT, Winegar BD, Kindler CH, Harada M, Taylor DM, Chavez RA, Forsayeth JR, and Yost CS. An open rectifier potassium channel with two pore domains in tandem cloned from rat cerebellum. *J Neurosci* 18: 868–877, 1998.
13. Lesage F and Lazdunski M. Molecular and functional properties of two-pore-domain potassium channels. *Am J Physiol Renal Physiol* 279: F793–F801, 2000.
14. Lopes CMB, Gallagher PG, Buck ME, Butler MH, and Goldstein SAN. Proton block and voltage gating are potassium-dependent in the cardiac leak channel Kcnk3. *J Biol Chem* 275: 16969–16978, 2000.
15. Lucchesi BR and Mullane KM. Leukocytes and ischemia-induced myocardial injury. *Annu Rev Pharmacol Toxicol* 26: 201–224, 1986.
16. Maingret F, Patel AJ, Lazdunski M, and Honore E. The endocannabinoid anandamide is a direct and selective blocker of the background K⁺ channel TASK-1. *EMBO J* 20: 47–54, 2001.
17. Massey CV, Kohout TA, Gaa ST, Lederer WJ, and Rogers TB. Molecular and cellular actions of platelet-activating factor in rat heart cells. *J Clin Invest* 88: 2106–2116, 1991.
18. Millar JA, Barratt L, Southan AP, Page KM, Fyffe R, Robertson B, and Mathie A. A functional role for the two-pore domain potassium channel TASK-1 in cerebellar granule neurons. *Proc Natl Acad Sci USA* 97: 3614–3618, 2000.
19. Montrucchio G, Alloati G, and Camussi G. Role of platelet-activating factor in cardiovascular pathophysiology. *Physiol Rev* 80: 1669–1699, 2000.
20. Mullane KM, Read N, Salmon JA, and Moncada S. Role of leukocytes in acute myocardial infarction in anesthetized dogs: relationship to myocardial salvage by anti-inflammatory drugs. *J Pharmacol Exp Ther* 228: 510–522, 1984.
21. Premkumar L and Ahern GP. Induction of vanilloid receptor channel activity by protein kinase C. *Nature* 408: 985–990, 2000.
22. Romson JL, Hook BG, Kunkel SL, Abrams GD, Schork MA, and Lucchesi BR. Reduction of the extent of ischemic myocardial injury by neutrophil depletion in the dog. *Circulation* 67: 1016–1023, 1983.
23. Shukla SD. Platelet-activating factor receptor and signal transduction mechanisms. *FASEB J* 6: 2296–2301, 1992.
24. Talley E, Lei Q, Sirois J, and Bayliss D. TASK-1, a two-pore domain K⁺ channel, is modulated by multiple neurotransmitters in motoneurons. *Neuron* 25: 399–410, 2000.
25. Toullec D, Pianetti P, Coste H, Bellevergue P, Grand-Perret T, Ajakane M, Baudet V, Boissin P, Boursier E, and Loriolle F. The bisindolylmaleimide GF 109203X is a potent and selective inhibitor of protein kinase C. *J Biol Chem* 266: 15771–15781, 1991.
26. Wahler GM, Coyle DE, and Sperelakis N. Effects of platelet-activating factor on single potassium channel currents in guinea pig ventricular myocytes. *Mol Cell Biochem* 93: 69–76, 1990.

Characterization of Mouse Cysteinyl Leukotriene Receptors mCysLT₁ and mCysLT₂

DIFFERENTIAL PHARMACOLOGICAL PROPERTIES AND TISSUE DISTRIBUTION*

Received for publication, October 1, 2001, and in revised form, February 15, 2002
Published, JBC Papers in Press, February 19, 2002, DOI 10.1074/jbc.M109447200

Hideaki Ogasawara^{‡§}, Satoshi Ishii^{‡§}, Takehiko Yokomizo^{‡§}, Takashi Kakinuma[¶],
Mayumi Komine[¶], Kunihiko Tamaki[¶], Takao Shimizu^{‡§||}, and Takashi Izumi^{§**}

From the Departments of [‡]Biochemistry and Molecular Biology and [¶]Dermatology, Faculty of Medicine, The University of Tokyo, Bunkyo-ku, Tokyo 113-0033, [§]CREST of Japan Science and Technology Corporation, Bunkyo-ku, Tokyo 113-0033, and the ^{**}Department of Biochemistry, Gunma University School of Medicine, Maebashi, Gunma 371-8511, Japan

Cysteinyl leukotrienes (LTs) are important proinflammatory mediators. Their precise roles in mice need to be elucidated to interpret mouse models of inflammatory diseases. For this purpose, we cloned and characterized mouse receptors for cysteinyl LTs, mCysLT₁ and mCysLT₂. mCysLT₁ and mCysLT₂ were composed of 339 amino acids with 87.3% identity and 309 amino acids with 73.4% identity to human orthologues, respectively. A pharmacological difference was noted between mouse and human CysLT₂. Pranlukast, a specific inhibitor for human CysLT₁, antagonized mCysLT₂ responses as determined by Ca²⁺ elevation and receptor-induced promoter activation. The mRNA expressions of both mCysLTs were higher in C57BL/6 mice than in 129 mice. mCysLT₁ mRNA was expressed mainly in skin, lung, and small intestine. mCysLT₂ was seen more ubiquitously with high expressions in spleen, lung, and small intestine. By *in situ* hybridization we demonstrated for the first time that mCysLT₁ and mCysLT₂ were expressed in subcutaneous fibroblasts. The different pharmacological characteristics of CysLT₂ between human and mouse and the different distributions of CysLTs between mouse strains suggest that careful choice and interpretation are necessary for a study of CysLTs using animal models.

Cysteinyl leukotrienes (LTs)¹ including LTC₄, LTD₄, and LTE₄ are inflammatory mediators previously known as SRS-A (slow reacting substances of anaphylaxis) (1–4). They are produced by LTC₄ synthase from the biologically inactive precursor LTA₄, a product of 5-lipoxygenation of arachidonic acid (5–7). LTC₄ synthase is expressed in inflammatory cells including mast cells, eosinophils, basophils, and monocytes/macro-

phages (7). The cysteinyl LTs are potent bronchoconstrictors and macrophage activators, and have been identified in urine and tissues in asthmatic patients (8–10). At least two cysteinyl LT receptors (CysLT₁ and CysLT₂) have been defined pharmacologically as G protein-coupled receptors. Most of the biological reactions of cysteinyl LTs including bronchospasm, plasma exudation, vasoconstriction, mucus secretion, and eosinophil recruitment are mediated through interaction with CysLT₁ (11). CysLT₁ antagonists, montelukast (SingulairTM) (12, 13), zafirlukast (AccolateTM) (14), and pranlukast (OnonTM) (15) are currently used clinically for the treatment of bronchial asthma and allergic rhinitis. Human CysLT₁, human CysLT₂, and mouse CysLT₁ were recently cloned and characterized (16–21). Human CysLT₁ mRNA was detected in airway smooth muscle cells, tissue macrophages, monocytes, and eosinophils (16, 17). Human CysLT₂ mRNA was prominently expressed in lung macrophages, airway smooth muscle, cardiac Purkinje cells, adrenal medulla cells, peripheral blood leukocytes, placenta, spleen, and brain (18–20).

Ovalbumin sensitization and aerosol challenge in mice elicits release of LTB₄ and LTC₄ into bronchoalveolar lavage fluid, eosinophilia in the mucosa and the bronchoalveolar lavage fluid, and increased airway reactivity to methacholine (22). Although cysteinyl LTs are not established as bronchoconstrictors in mice, MK-571, a CysLT₁-selective antagonist, inhibits eosinophilia, bronchial hyperreactivity, and microvascular leakage of mice (23), suggesting a contribution of cysteinyl LTs in these processes. We cloned and characterized the mouse CysLT₁ (mCysLT₁) and CysLT₂ (mCysLT₂) to better study the roles of cysteinyl LTs in animal models of diseases.

MATERIALS AND METHODS

Antagonists—Pranlukast was a generous gift from Ono Pharmaceutical Co. (Osaka, Japan). MK-571 and BAY u9773 were purchased from BIOMOL Research Laboratories (Plymouth Meeting, PA). Pranlukast and MK-571 were dissolved in 100% ethanol to make 10 mM stock solutions.

Cloning and Expression of mCysLT₁ and mCysLT₂—A mouse genome library (129 inbred strain) in λFix II vector (Stratagene, La Jolla, CA) was screened with [³²P]dCTP-labeled partial open reading frame (ORF) of human CysLT₁ (581 nucleotides), and a clone was isolated. The CysLT₁ ORF from C57BL/6 was obtained by PCR with a genome template using sense (5'-ATTCTGGGAGAACATGAATGG-3') and antisense (5'-CATTGTTCTGCACTGTAGATGAG-3') primers. A mouse expressed sequence tag clone with 88.4% identity in cDNA sequence to the human CysLT₁ was found during a routine BLAST search of the NCBI data base (GenBankTM accession number AI506060), and it was purchased from Genome Systems (St. Louis, MO). These three clones were sequenced using an automated DNA sequencer 373A (Applied Biosystems, Foster City, CA) and found to be completely identical. The ORF of the expressed sequence tag clone was amplified by PCR with

* The work was supported in part by Grants-in-aid from the Ministry of Education, Culture, Sports, Science and Technology of Japan and grants from the Yamanouchi Foundation for Metabolic Disorders and the ONO Medical Research Foundation. The costs of publication of this article were defrayed in part by the payment of page charges. This article must therefore be hereby marked "advertisement" in accordance with 18 U.S.C. Section 1734 solely to indicate this fact.

The nucleotide sequence(s) reported in this paper has been submitted to the GenBankTM/EBI Data Bank with accession number(s) AB044087 and AB058930.

|| To whom correspondence should be addressed. Tel.: 81-3-5802-2925; Fax: 81-3-3813-8732; E-mail: tshimizu@m.u-tokyo.ac.jp.

¹ The abbreviations used are: LT, leukotriene; CHO, Chinese hamster ovary; FCS, fetal calf serum; G3PDH, glyceraldehyde-3-phosphate dehydrogenase; HEK, human embryonic kidney; ORF, open reading frame; PBS, phosphate-buffered saline; m, mouse; AM, acetoxymethyl; TM, transmembrane domain.

